Food Research International 173 (2023) 113295

Contents lists available at ScienceDirect

Food Research International

journal homepage: www.elsevier.com/locate/foodres

Evaluation of berberine nanoparticles as a strategy to modulate acetylcholinesterase activity

Fernanda Vitória Leimann [a,b,1,*], Luma Borges de Souza [a], Byanca Pereira Moreira de Oliveira [c], Bruna Franzon Rossi [c], Patrícia Sabino da Silva [d], Carlos Seiti Hurtado Shiraishi [b,e], Vanessa Kaplum [a], Rui Miguel Abreu [b,e], Carla Pereira [b,e], Lillian Barros [b,e], Ana Paula Peron [f], Rafael Porto Ineu [g], Bruno Francisco Oechsler [h], Claudia Sayer [h], Pedro Henrique Hermes de Araújo [h], Odinei Hess Gonçalves [a,b,*]

[a] Post-Graduation Program of Food Technology (PPGTA), Federal University of Technology – Paraná – UTFPR, Brazil
[b] Centro de Investigação de Montanha (CIMO), Instituto Politécnico de Bragança, Campus de Santa Apolónia, Bragança, Portugal
[c] Food and Chemical Engineering Academic Department (DAAEQ), Federal University of Technology – Paraná – UTFPR, Brazil
[d] Department of Chemical Enginneering, State University of Maringá – UEM, Brazil
[e] Laboratório Associado para a Sustentabilidade e Tecnologia em Regiões de Montanha (SusTEC), Instituto Politécnico de Bragança, Campus de Santa Apolónia, 5300-253 Bragança, Portugal
[f] Biodiversity and Nature Conservation Department, Federal University of Technology – Paraná – UTFPR, Brazil
[g] Department of Technology and Food Science, Federal University of Santa Maria - UFSM, Brazil
[h] Department of Chemical Engineering and Food Engineering, Federal University of Santa Catarina, Brazil

ARTICLE INFO

Keywords:
Solid dispersion
Encapsulation
AChE
Kinetic
Bioactive
Berberis vulgaris

ABSTRACT

Researchers have concentrated efforts in the search for natural-based reversible inhibitors for cholinesterase enzymes as they may play a key role in the treatment of degenerative diseases. Diverse plant alkaloids can inhibit the action of acetylcholinesterase and, among them, berberine is a promising bioactive. However, berberine has poor water solubility and low bioavailability, which makes it difficult to use in treatment. The solid dispersion technique can improve the water affinity of hydrophobic substances, but berberine solid dispersions have not been extensively studied. Safety testing is also essential to ensure that the berberine-loaded solid dispersions are safe for use. This study investigated the effectiveness of berberine-loaded solid dispersions (SD) as inhibitors of acetylcholinesterase enzyme (AChE). Docking simulation was used to investigate the influence of berberine on AChE, and *in vitro* assays were conducted to confirm the enzymatic kinetics of AChE in the presence of berberine. Berberine SD also showed improved cytotoxic effects on tumoral cells when dispersed in aqueous media. In vivo assays using Allium cepa were implemented, and no cytotoxicity/genotoxicity was found for the berberine solid dispersion. These results suggest that berberine SD could be a significant step towards safe nanostructures for use in the treatment of neurodegenerative diseases.

1. Introduction

Berberine is an isoquinoline alkaloid found in plants of the Euphorbiaceae, Ranunculaceae, and Papaveraceae families (Gao et al., 2020; Sarraf et al., 2019) and also found in the roots of *Berberis* species, such as *B. vulgaris* (Imenshahidi & Hosseinzadeh, 2019; Sarraf et al., 2019). A wide range of pharmacological activities is already documented for berberine, including the action on cancer cells, metabolic disorders, and cardiovascular diseases (Gao et al., 2020; Liu et al., 2019a, 2019b).

Berberine was also reported for the treatment of neurodegenerative diseases, such as Alzheimer's, Parkinson's, and Huntington's diseases (Fan et al., 2019; Lin & Zhang, 2018). Alzheimer's disease (AD) is a progressive brain condition that results in memory impairment, and cognitive skills decline is known to be the major cause of dementia (Long

* Corresponding authors.
E-mail addresses: fernandaleimann@utfpr.edu.br (F.V. Leimann), odinei@utfpr.edu.br (O.H. Gonçalves).
[1] Full postal address: Post-Graduation Program of Food Technology (PPGTA), Federal University of Technology – Paraná – UTFPR, Campo Mourão, via Rosalina Maria dos Santos, 1233, CEP 87301-899, Campo Mourão, PR, Brazil.

https://doi.org/10.1016/j.foodres.2023.113295
Received 5 April 2023; Received in revised form 13 July 2023; Accepted 19 July 2023
Available online 20 July 2023

& Holtzman, 2019). The cholinergic hypothesis is one of the most accepted theories to understand the causes of AD, linking it to the deficiency in brain acetylcholine levels (Liu et al., 2019a, 2019b). Acetylcholine concentration may be modulated by cholinesterase inhibitors, a strategy used by some drugs approved for AD treatment, such as donepezil, galantamine, and rivastigmine (Yiannopoulou & Papageorgiou, 2020). Berberine is a promising treatment for AD due to various mechanisms, including a significant inhibition of acetylcholinesterase (Cai et al., 2016; Fan et al., 2019; Singh et al., 2019). Several works have already reported the neuroprotective activity of berberine in animal models of AD (Yuan et al., 2019).

Understanding the kinetic mechanism and the reactions between berberine and acetylcholinesterase is of key importance to developing safe and optimized therapeutic applications. Also, this approach may provide valuable information at the molecular level on the interaction of ligands with the corresponding protein (Rasoulzadeh et al., 2009). One of the most common procedures used to determine the kinetic constant of inhibition is the linear transformation procedure, or double-reciprocal method of plotting kinetic data, the Lineweaver–Burk plot (reciprocal rate versus reciprocal substrate). However, the most common misuse of this method is to take a nonlinear equation, rearrange it to a linear form, and then perform linear regression to fit data without any consideration regarding the error propagation involved in the rearrangements of the original variables. In this sense, the statistical inference of kinetic parameters uncertainty is compromised, since the uncertainty of experimental variables in linear form is unknown (Aledo & Juan Aledo, 2021). The particle swarm optimization (PSO) algorithm is a heuristic optimization method, based on empirical evolutionary rules that frequently mimic successful optimization strategies found in nature, that can be successfully applied in non-linear parameter estimation procedures and computation of likelihood parameter confidence regions (Schwaab et al., 2008).

Although presenting remarkable bioactivity, berberine shows poor aqueous solubility that may impact membrane permeability and bioavailability (Mirhadi et al., 2018). Several nanoparticle-based delivery systems for berberine have been proposed to improve aqueous affinity and bioavailability (Chenthamara et al., 2019; Ma et al., 2013; Majidzadeh et al., 2020; Xue et al., 2013, 2015). Solid dispersions are complex systems used in diverse applications in the pharmaceutical, chemical and food industries. In the pharmaceutical field, amorphous solid dispersions are composed of an active pharmaceutical ingredient inside an amorphous solid material, often a polymeric matrix (Huang & Dai, 2014; Schittny et al., 2020). Excellent reviews are available in the literature demonstrating the gains in solubility, bioavailability, and water affinity of solid dispersions (Dumortier et al., 2006; Y. Huang & Dai, 2014; Jaskirat et al., 2011; Schittny et al., 2020). Several polymers may be used as the encapsulant matrix, and poly(ethylene oxide)-poly (propylene oxide) (PEO-PPO) block copolymers are a suitable choice to facilitate the solubilization of poorly water-soluble molecules (Dumortier et al., 2006). Berberine-loaded solid dispersions were reported in the literature with phospholipid from soy lecithin (Zhang et al., 2014b), polyvinylpyrrolidone, polyethylene glycol, and poloxamer 188, a PEO-PPO-PEO block copolymer (Zhaojie et al., 2014) or β-cyclodextrin (Y. Zhang et al., 2013). It is worth noting that the use of polysorbate 80 and polymers of the poloxamer family is preferable since these substances are known to facilitate the permeation of the nanoparticles through the blood–brain barrier (Joseph et al., 2021; Kreuter, 1996; Kulkarni & Feng, 2011) which is crucial in the case of acetylcholinesterase modulation.

Solid dispersions are already in use in the pharmaceutic field, showing low toxicity and even a decrease in toxicity levels (Bikiaris et al., 2009), but case by case studies are a demand of both academia and consumers due to increasing concerns about how nanotechnology could affect the human body in short and long terms. An initial pre-clinical toxicity analysis can be performed using cell-based *in vitro* cytotoxicity methodologies, and the most common cell-based approaches include cell viability assays of different cell lines when exposed to different samples. Also, *in vivo* experiments may give insight into the toxicity of nanoengineered systems. Assays using *Allium cepa* L. root meristems are internationally accepted for toxicogenetic tests because the results obtained through this bioassay can be extrapolated to other eukaryotic organisms since the cellular control of interphase and mitosis are very similar between them (Bonciu et al., 2018). In fact, A. cepa is established as a routine test that correlates well with mammalian test systems (Bonciu et al., 2018; Herrero et al., 2012; Pandey et al., 2014). The intense cell proliferation that occurs in the meristematic region of its roots allows the evaluation of the cell cycle, mitotic spindle alterations, and chromosomal breaks (Ventura-Camargo et al., 2016). These tests also correlate satisfactorily to the results of genetic tests carried out in other bioassays, such as those with cell culture (Herrero et al., 2012; Sales et al., 2017). The biomarkers used for the evaluation of cytotoxicity and genotoxicity are the mitotic index and the frequency of chromosome/mitotic spindle changes, respectively (Herrero et al., 2012; T. de S. Silva et al., 2020). A. cepa was already used to assess the chromosomal aberrations and lipid peroxidation eventually caused by nanoparticles and nanostructures (Ahmed et al., 2017; Rheder et al., 2018).

Reversible cholinergic inhibitors are in great need and nanotechnology may play a key role in improving the action of natural-based substances, and berberine was reported to be a potent acetylcholinesterase inhibitor (Abd El-Wahab et al., 2013; Ji & Shen, 2011). Recent efforts to have concentrated in finding new molecular derivatives of berberine (Koly et al., 2023), nanoparticles (Salehi et al., 2019) or liposome encapsulation (Wang et al., 2023), and research has concentrated mainly in *in vitro* and rats *in vivo* models. The present study aimed to investigate the action of a berberine-loaded solid dispersion on the activity of the acetylcholinesterase enzyme. A comparison was performed between the inhibition kinetic parameters estimated by Lineweaver–Burk plot and by non-linear parameter estimation procedures and by using a hybrid optimization method combining particle swarm optimization (PSO) and Gauss–Newton algorithms. The likelihood confidence regions of kinetic parameters were computed and model discrimination was performed for the acetylcholinesterase inhibition by berberine in its free and solid dispersion forms. Furthermore, the interaction of free berberine with AChE was explored by the docking strategy.

2. Material and methods

2.1. Material

The following reagents were used for the solid dispersion production: berberine (90%, Sigma-Aldrich), Kolliphor® Poloxamer 407 (encapsulant, 12,000 g/mol, Sigma-Aldrich), Tween 80 (Dinâmica) and ethanol (99.8%, Neon). All chemicals were of analytical grade and purchased from common sources unless otherwise mentioned. The following reagents were used for the AChE activity assay: acetylcholinesterase (AChE; E.C. 3.1.1.7 from electric eel, Sigma-Aldrich)), 5′,5-dithiobis(2-nitrobenzoic acid) (DTNB; 98%, Sigma-Aldrich), acetylthiocholine iodide (ASCh; 99%, Sigma-Aldrich), and potassium phosphate buffer (TFK; pH 7.5, Neon). Potassium bromide (spectroscopic standard, Sigma-Aldrich) was used in the infrared spectra analyses. Trichloroacetic acid (TCA), 6-hydroxy-2,5,7,8-tetramethylchroman-2-carboxylic acid (Trolox) and 2,2′-azobis(2-methylpropionamidine) dihydrochloride (AAPH) (from Sigma-Aldrich) were used in the oxidative hemolysis inhibition assay (OxHLIA) and thiobarbituric acid reactive substances (TBARS) assays. Acetic acid, sulforhodamine B (SRB), ellipticine, dexamethasone, trypan blue, lipopolysaccharide (LPS), tris-(hydroxymethyl) aminomethane (TRIS) (from Sigma-Aldrich), dimethyl sulfoxide (DMSO) (from Fisher Scientific), Dulbecco's Modified Eagle's Medium (DMEM) and RPMI-1640 medium, fetal bovine serum (FBS), Hank's balanced salt solution (HBSS), L-glutamine, nonessential amino

acid solution (2 mmol/L), penicillin/streptomycin solution (100 U.mL^{-1} and 100 mg mL^{-1}, respectively), trypsin and EDTA (from Hyclone) were used in the cytotoxic and anti-inflammatory activity assays. Ethanol, acetic acid, and distilled water were used in the cytotoxic and genotoxic analyses. Methanesulfonate (MMS) was used as positive control, and onion bulbs (*Allium cepa* L, variety beta crystal) was selected from an organic garden. The purified acetylcholinesterase was purchased directly from Sigma-Aldrich, not involving manipulation of animals or parts of animals, tissues, or other derivatives. The blood used for the OxLHIA assay was obtained randomly from the normal blood analysis of the animals and not directly for the assay.

2.2. Solid dispersion production and physicochemical characterization

The berberine-loaded solid dispersion was produced according to Sá et al. (2019) with minor modifications. Poloxamer 407 (1.200 g), a PEO-PPO-PEO block copolymer, and Tween 80 (0.012 g), a PEO sorbitan monooleate, were added to ethanol (50 mL) and mixed under gentle stirring for 10 min. Then, berberine (0.120 g) was added and mixed for 5 min. The dispersion was sonicated (Fisher Scientific, 120 W, 1/8′ probe) for 3 min under a pulse regime (30 s on and 10 s off) in an ice bath. Ethanol was evaporated in a forced air circulation oven at 40 °C for 24 h and the resulting powder was stored at −10 °C protected from light.

The interaction between Poloxamer and berberine was quantitatively evaluated by UV–Vis spectroscopy (OceanOptics, Red Tide USB 650 UV) as reported by Karavas et al. (2006). Ethanol was used as a solvent and different amounts of the two components were added (mass proportions from 1:1 to 20:1 Poloxamer:berberine). Solutions were obtained in triplicate and absorbance at 350 nm was used to calculate the normalized interaction coefficient (Equation (1), where A and A_0 were the maximum absorbance at 350 nm for the solutions and an ethanolic solution of berberine alone. It is worth noting that Poloxamer 407 do not present absorbance at 350 nm (Butt et al., 2015)and the changes in the absorbance of berberine may be accounted for changes in the molar extinction coefficient caused by possible interactions between berberine and Poloxamer 407 (Karavas et al., 2006).

$$F = \frac{A - A_0}{A_0} \tag{1}$$

The thermal properties of the solid dispersion were analyzed by Differential Scanning Calorimetry (DSC, Perkin Elmer 4000) and samples were heated in aluminum pans (0 °C to 350 °C at 10 °C.min^{-1}) under nitrogen flow (100 mL.min^{-1}). Fourier Transform Infrared spectra (FTIR; Frontier Perkin Elmer) was performed in potassium bromide pellets with a resolution of 2 cm^{-1} from 4500 to 425 cm^{-1} with 32 cumulative scans. Transmission electron microscopy (TEM; JEOL model JEM 2100, 200 kV) was performed to observe the morphology of the nanoparticles in parlodium-covered copper grids (300 mesh). In addition, a mixture of berberine and Poloxamer 407 was obtained by simply mixing them in a laboratory mortar in the same mass proportion found in the solid dispersion. The objective was to compare this physical mixture with the berberine-loaded solid dispersion (Almeida et al., 2018; Sá et al., 2019).

2.3. In vitro cytotoxicity, antioxidant and anti-inflammatory activity

To assess the cytotoxicity of the sample, the sulforhodamine (SRB) assay was performed according to a procedure previously established by Abreu et al. (2011) in triplicate (n = 3). Berberine was dissolved in water:DMSO (1:1 vol) and berberine-loaded solid dispersion was dispersed in water, both at the same concentration of berberine (8 mg.mL^{-1}), and this stock solution was used to prepare successive dilutions. CaCo cell line, MCF-7 (breast adenocarcinoma), NCIH460 (non-small cell lung carcinoma), and VERO cells from DSMZ (Leibniz-Institute DSMZ - German Collection of Microorganisms and Cell Cultures) were selected as human tumour cell lines. Porcine liver cells (PLP2), a primary cell culture, were prepared according to the procedure described by Abreu et al. (2011). These cells were treated for 48 h with the different sample solutions and the SRB assay was followed (Souza et al., 2015). Ellipticine was used as a positive control. The results were expressed as GI_{50} values (concentration that inhibited 50% of the net cell growth).

The antihemolytic activity (OxHLIA) was assessed using the method described by Takebayashi et al. (2012) as fully described in previous work (Sá et al., 2019). Briefly, sheep blood samples were collected from healthy animals and centrifuged at 1,000*g* for 5 min at 10 °C. Plasma and buffy coats were discarded and erythrocytes were firstly washed once with NaCl solution (150 mmol/L) and three times with phosphate-buffered saline solution (PBS, pH 7.4) (Evans et al., 2013). The erythrocyte pellet was then resuspended in PBS at 2.8% (v/v). Using a flat-bottom 48-well microplate, 200 μL of erythrocyte solution was mixed with 400 μL of either PBS solution (control) and was dispersed in PBS, or water (for complete hemolysis). After pre-incubation at 37 °C for 10 min with shaking, AAPH (200 μL, 160 mmol/L in PBS) was added and the optical density was measured in a microplate reader (Bio-Tek Instruments, ELX800) at 690 nm. After that, the microplate was incubated under the same conditions and the optical density was measured every 10 min at the same wavelength for approximately 300 min. The percentage of the erythrocyte population that remained intact (*P*) was calculated by Equation (2) (S_t and S_0 correspond to the optical density of the sample at *t* and 0 min, respectively, and CH_0 is the optical density of the complete hemolysis at 0 min).

$$P\% = 100\left(\frac{S_t - CH_0}{S_0 - CH_0}\right) \tag{2}$$

Results were expressed as the delayed time of hemolysis (Δt), calculated by Equation (3), where Ht_{50} is the 50% hemolytic time (min) graphically obtained from the hemolysis curve of each sample concentration. The Δt values were then correlated to the different sample concentrations (Takebayashi et al., 2012) and the concentration able to promote a Δt hemolysis delay was calculated. The results were expressed as IC_{50} values (μg.mL^{-1}) at Δt 60 and 120 min, i.e. the sample concentration required to keep 50% of the erythrocyte population intact for 60 and 120 min. Trolox was used as a positive control and all experiments were carried out in triplicate (n = 3).

$$\Delta t(min) = \frac{Ht_{50}(sample)}{Ht_{50}(control)} \tag{3}$$

The capacity of the sample to inhibit the formation of thiobarbituric acid reactive substances (TBARS), such as malondialdehyde generated from the *ex vivo* decomposition of lipid peroxidation products, was evaluated using porcine brain cell homogenates, following the method described previously (Pinela et al., 2012). Trolox was used as the positive control. The results were expressed as IC_{50} values (μg.mL^{-1}), i.e. the sample concentration providing 50% of antioxidant activity and all experiments were carried out in triplicate (n = 3).

For the anti-inflammatory activity determination (Sobral et al., 2016), the lipopolysaccharide (LPS)-induced nitric oxide (NO) production by a murine macrophage (RAW 264.7) cell line was quantified as nitrite concentration in the culture medium. The effect of the tested compounds in the absence of LPS was also evaluated, to observe if they induced changes in NO basal levels. In negative controls, no LPS was added. For the NO determination, a Griess Reagent System kit containing sulfanilamide, N-1-naphthyl ethylenediamine dihydrochloride (NED), and nitrite solutions were used. Dexamethasone was used as a positive control. The results were expressed as IC_{50} values (μg.mL^{-1}), i.e. compound concentration providing 50% of NO production inhibition and all experiments were carried out in triplicate (n = 3).

2.4. Cytotoxic and genotoxic analysis of berberine in Allium cepa L

The experiments were carried out as previously described in details

by Fiskesjo (1985) and Sales et al., 2017. It is worth noting that the amount of the solid dispersion used in the experiments was adjusted to represent the same berberine concentration in the cases where free berberine was used. For the assessment of cytotoxicity and genotoxicity of berberine and the berberine-loaded solid dispersion, the onion bulbs were placed in vials with distilled water, constantly aerated, to obtain roots of 2.0 cm in length. For analysis of berberine and Poloxamer concentrations (treatments), an experimental group with five onion bulbs was set up. Before putting the roots in contact with their respective treatments, some roots were collected and fixed to serve as a control of the bulb itself, which was identified as the time of analysis of 0 h or control of the bulb itself (Co − 0 h). Then, the other roots were put in their respective treatments for 24 and 48 h, procedures called exposure times 24 and 48 h, where roots were collected every 24 h. Positive control was prepared with methyl methanesulfonate (MMS), a known cytotoxic and genotoxic substance to the *A. cepa* test system, at the concentration $4x10^{-4}$ mol.L^{-1}. All roots collected during the experiment were fixed in 3:1 Carnoy solution (ethanol: acetic acid) for up to 24 h. Glass slides were prepared according to the protocol proposed by Herrero et al. (2012) and analyzed under an optical microscope with a 40x objective lens. For each bulb, 1,000 cells were analyzed, totaling 3,000 cells for each control group (0 h), each group exposure time 24 h and each group exposure time 48 h, totaling 9,000 cells analyzed for each concentration of treatments. For the MMS group 3000 cells were analyzed in five independent experiments.

For estimates of the mitotic index, cells in interphase, prophase, metaphase, anaphase, and telophase were counted to determine the cytotoxic potential. The mitotic index (MI) or cell division index was calculated by Equation (4).

$$MI = 100 \times \frac{\text{total number of dividing cells}}{\text{Total number of cells analyzed}} \quad (4)$$

The genotoxic potential was assessed by determining the number of cell alterations such as micronuclei, colchicine metaphases, anaphase and telophase bridges, cells with adhesions, nuclear buds and multipolar anaphases.

2.5. Enzyme activity assays

AChE activity assay and reaction kinetics. The determination of the acetylcholinesterase (AChE) activity was performed according to modifications in the methods of Ellman et al. (1961) and Pereira et al. (2004). In 96-well plate, the following reagents were pre-incubated for 10 min at 25 °C: TFK (90 μL; 50 mmol/L), water (45 or 55 μL), AChE (15 μL; 0.09 U/mL) and different dilutions of **(1)** berberine (10 μL; 0.03, 0.1, 0.3, 1 and 3 μmol/L) or different dilutions of **(2)** berberine-loaded solid dispersion (10 μL; 0.03, 0.1, 0.3, 1 and 3 μmol/L). The control group was incubated with water. After incubation, DTNB (20 μL; 0.2 mmol/L) and acetylthiocholine iodide (ASCh; 20 μL; 800 μmol/L) were added. Absorbance was read at 412 nm for 4 min every 60 s using a Vis spectrophotometer (Thermoplate TP-Reader). The concentration that inhibited AChE activity in 50% (IC_{50}) compared with the control (H_2O curve) was determined by nonlinear regression analysis.

Enzyme kinetic analysis was performed according to modifications in the methods described by Grella Miranda et al. (2020a). As in the AChE activity assays, the following reagents were pre-incubated for 10 min at 25 °C: TFK, ultrapure water, enzyme (AChE or S1), and different dilutions of **(1)** berberine or **(2)** berberine-loaded nanoparticles. The control group was incubated with water. After incubation, DTNB and different concentrations of ASCh (0, 25, 50, 100, 400 and 800 μmol/L) or BSCh (0, 25, 50, 100, 400 and 800 μmol/L) were added. Absorbance was read at 412 nm for 4 min every 60 s using a Vis spectrophotometer (Thermoplate TP-Reader).

Reaction kinetics modeling. The kinetic constants of the enzyme inhibition reactions were determined by different strategies: i) Docking simulations; ii) The Lineweaver-Burk reciprocal plot; iii) Non-linear parameter estimation using the Particle Swarm Optimization coupled with the Gauss-Newton algorithm.

(i) *Docking simulations.* 2D and 3D optimizations of Berberine structure were performed using Marvin Sketch 16.4 software (https://www.chemaxon.com). AutoDockTools 1.5.2 (ADT) was then used to convert the 3D structure of Berberine to the PDBQT file format (Eberhardt et al., 2021). The X-ray crystal structure of AChE (PDB: 6G1U) was obtained from the Protein Data Bank (PDB) (https://www.rcsb.org). The co-crystallized ligand was extracted from each PDB file, and ADT was used to assign polar hydrogens, add Gasteiger charges, and save the AChE structures in the required PDBQT file format (Grella Miranda et al., 2020a). Autodock Vina 1.2 (Eberhardt et al., 2021) was then used to perform molecular docking. An XYZ grid size of 30 by 30 by 30 Å was used for all structures with an exhaustiveness parameter of 16. The XYZ coordinates used for each structure were the following: 6ESY (3.6, −12.7, −12.3) and 6G1U (3.7; −4.5; 20.9). The predicted *Ki* (inhibition equilibrium constant) was calculated as follows: $Ki = \exp((\Delta G.1000)/(Rcal.TK))$ where ΔG is the predicted binding energy (cal/mol), Rcal is 1.98719 cal/(mol.K), and TK is 298.15 K. Structure representations were prepared using PyMOL (The PyMOL Molecular Graphics System, Version 1.3, Schrödinger, LLC).

(ii) *The Lineweaver-Burk reciprocal plot.* The Lineweaver-Burk method was applied using the classical equations described by Besswanger (2008). This method applies a linear transformation to the inhibition kinetic models and is largely applied to enzymatic kinetic data. The following linearized models were considered for evaluation: a) Competitive inhibition (Equation (5); b) Uncompetitive inhibition (Equation (6); c) Mixed Non-competitive inhibition (Equation (7); d) Pure Non-competitive inhibition (Equation (8), where Vmax is the maximum reaction rate (μmol/L/min/U); Km is the Michaelis constant (μmol/L); [S] is the substrate concentration (μmo/L); [I] is the inhibitor (pure berberine or nanoencapsulated berberine) concentration (μmol/L); while K_{ic} (competitive), K_{iu} (uncompetitive) and K_i are inhibition equilibrium constants (μmol/L).

$$\frac{1}{v} = \frac{1}{Vmax} + \frac{Km.\left(1 + \frac{[I]}{K_{ic}}\right)}{Vmax.[S]} \quad (5)$$

$$\frac{1}{v} = \frac{\left(1 + \frac{[I]}{K_{iu}}\right)}{Vmax} + \frac{Km}{Vmax.[S]} \quad (6)$$

$$\frac{1}{v} = \frac{\left(1 + \frac{[I]}{K_{iu}}\right)}{Vmax} + \frac{Km.\left(1 + \frac{[I]}{K_{ic}}\right)}{Vmax.[S]} \quad (7)$$

$$\frac{1}{v} = \frac{\left(1 + \frac{[I]}{K_{i}}\right)}{Vmax} + \frac{Km.\left(1 + \frac{[I]}{K_{i}}\right)}{Vmax.[S]} \quad (8)$$

(i) *Non-linear parameter estimation.* Non-linear parameter estimation was performed using a hybrid optimization method, which combines the particle swarm optimization (PSO) algorithm (a heuristic optimization method, based on empirical evolutionary rules that frequently mimic successful optimization strategies found in nature), and Gauss-Newton algorithms (Schwaab et al., 2008). This approach was used for the computation of likelihood parameter confidence regions. The same kinetic models described in the previous section were considered in their non-linear form for parameter estimation, Equations (9) for Michaelis-Menten, (10) for the competitive model, (11) for the uncompetitive model, (12) for the non-competitive mixed model, and (13) for the non-competitive pure model, except for the inclusion of the

Michaelis-Menten equation for analysis of kinetic data without the addition of an inhibitor. Furthermore, in this case, the parameters "a" and "b" that represent the factor with which Km and Vmax are multiplied to calculate the apparent constants in the presence of the inhibitor (Sharma, 2012).

$$v = \frac{V_{max}.[S]}{Km + [S]} \tag{9}$$

$$v = \frac{V_{max}.[S]}{b.Km.\left(1 + \frac{[I]}{kic}\right) + [S]} \tag{10}$$

$$v = \frac{a.V_{max}.[S]}{b.Km + [S].\left(1 + \frac{[I]}{kiu}\right)} \tag{11}$$

$$v = \frac{a.V_{max}.[S]}{Km.\left(1 + \frac{[I]}{kic}\right) + [S].\left(1 + \frac{[I]}{kiu}\right)} \tag{12}$$

$$v = \frac{a.V_{max}.[S]}{Km.\left(1 + \frac{[I]}{ki}\right) + [S].\left(1 + \frac{[I]}{ki}\right)} \tag{13}$$

The absorbance data measured in the kinetic assay was firstly used to calculate the reaction rate (v, μM/min/U) for each time interval (1, 2, 3, and, 4 min) with Equation (14) where: ΔAbs is the absorbance variation during the evaluated time interval (Δt, min); V_W is the volume of the reaction media in the well (μL); l represents the optic path (cm); ε-represents the molar extinction coefficient of DTNB (L/mol.cm); and V_E is the volume of enzyme solution in the reaction media (μL). After that, the data was submitted to the interpolation procedure in Matlab (R2021a) by the piecewise cubic Hermite interpolating polynomials (PCHIP), which was done using MATLAB's pchip function (Creasy et al., 2015) to determine the initial reaction rate at approximately 0.2 min. These results were used in the PSO procedure.

$$v = \frac{\Delta Abs.V_w.l}{\Delta t.\varepsilon.V_E} \tag{14}$$

The interpolated reaction rate results were submitted to the hybrid optimization method using Spyder (4.2.5) with Python (3.8). This computational code is based on ESTIMA, developed by Schwaab et al. (1993) originally for FORTRAN, which employs a hybrid estimation method that combines the particle swarm optimization method with a Gauss-Newton procedure, and also performs the statistical analysis of results. The following conditions were applied for parameter estimation: confidence level of 95%, 100 particles, and a maximum number of interactions equal to 100.

The weighting least squares function was considered the objective function (Fobj) to be minimized (maximum likelihood method), as described in Equation (15):

$$F_{obj} = \sum_{i=1}^{NE}\sum_{j=1}^{NY}\frac{\left(\boldsymbol{y}_{ij}^{e} - \boldsymbol{y}_{ij}^{m}\right)\left(\boldsymbol{x}_{i}^{m}, \boldsymbol{\theta}\right)}{\sigma_{ij}^{2}} \tag{15}$$

where NE is the number of experiments, NY is the number of output variables, $\boldsymbol{y}_{ij}^{e}$ is the vector of experimental values for the output variable, $\boldsymbol{y}_{ij}^{m}$ is the vector of the predicted values for the output variables, $\boldsymbol{x}_{i}^{m}$ is the vector of input variables, $\boldsymbol{\theta}$ is the parameter cluster, and σ_{ij}^{2} is the experimental variance.

For the model discrimination, the Chi^2 test was applied and the models were considered proper when the objective function was found within the Chi^2 range. In addition, the quality of the estimated model parameters was evaluated concerning the Likelihood confidence region and graphics comparing experimental and predicted results.

2.6. Statistical analyses of the experimental results

For the cytotoxic and genotoxic analysis in *Allium cepa* L., data represented in the graphs are expressed as the mean ± standard deviation of three independent experiments, and means were compared by the Scott-Knott test at 0.05 significance. In the enzymatic experiments, data represented in the graphs are expressed as the mean ± standard deviation of at least three independent experiments. Data were analyzed using one- or two-way analysis of variance (ANOVA) followed by Tukey's *post hoc* test. Values of $p \leq 0.05$ were considered statistically significant. The statistical analysis was performed using Prism GraphPad 5.0 software or Statistica 7.0 software.

3. Results and discussion

3.1. Nanoparticles characterization

The interaction between berberine and the encapsulant Poloxamer 407 was evaluated by UV–Vis spectroscopy to find the optimal amount of berberine to be encapsulated (Fig. 1). Then, the berberine solid dispersion was obtained and characterized. Fig. 2 presents the Transmission Electron Microscopy image and Fig. 3 shows the Differential Scanning Calorimetry thermogram, and the Infrared spectra of the nanoparticles.

It is worth noting that the interaction factor is a quantitative measure of the hyperchromic effect which occurs when chemical changes lead to an increase in the molar extinction coefficient for a particular chromophore group. Since Poloxamer does not present absorbance at 350 nm (Butt et al., 2015), the changes in absorbance may not be accounted for by the increasing concentration of poloxamer in the solutions. The increase in absorbance observed in Poloxamer:berberine solutions may be attributed to chemical interactions between the polymer and berberine, mostly by the formation of hydrogen bonds between hydroxyl and carbonyl groups. Interactions increased more sharply when the amount of Poloxamer increased, and then the value stabilized around 10:1 Poloxamer:berberine mass proportion. This value was chosen to be used in the nanoparticles obtention. The hyperchromic effect was also observed by Desai, Poddar and Sawant (2016) due to eslicarbazepine acetate complexation with β-cyclodextrin and for lutein and polyvinylpyrrolidone (Silva et al., 2017a, 2017b).

The berberine-loaded solid dispersion presented nanoparticles with irregular shapes and with sizes around 50–100 nm (indicated by arrows in the Fig. 2). The formation of nanoparticles from solid solutions containing natural-based bioactives was reported for curcumin, lutein and betacarotene by our research group (Almeida et al., 2018; Freitas et al.,

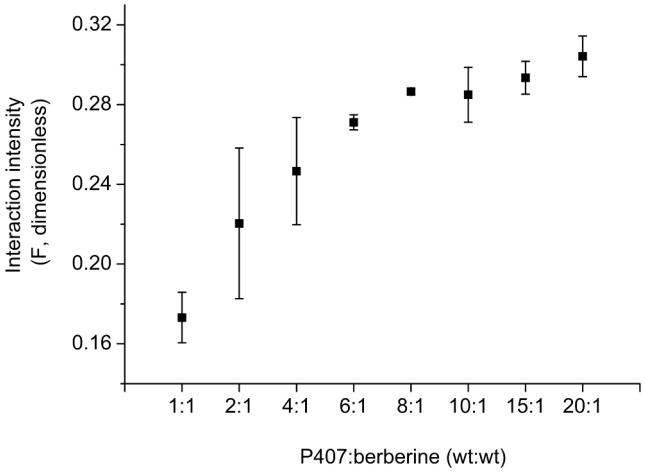

Fig. 1. Interaction intensity (F) between Poloxamer 407 and berberine as determined by UV–Vis Spectroscopy.

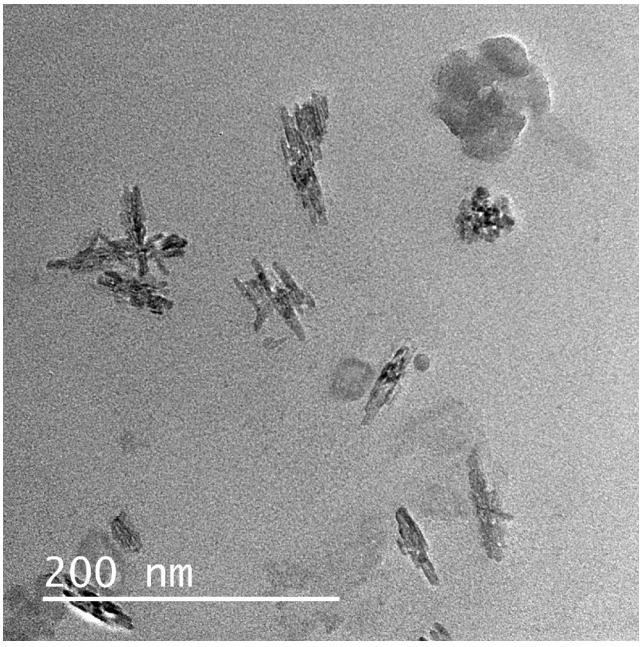

Fig. 2. Transmission Electron Microscopy image of the berberine-loaded solid dispersion.

2019; Grella Miranda et al., 2020b; Rocha et al., 2018; Santos et al., 2020; Silva et al., 2017a, 2017b). Based on the DSC curves, the melting peaks of P407 and berberine were 55 °C and 99 °C, respectively. Berberine showed an endothermic peak at 196 °C, with another exothermic peak at 200 °C and degradation may be observed at 288 °C. Battu et al. (2010) also reported an endothermic peak for berberine at 196 °C. An intense fusion peak for berberine was also shown at 99 °C (Pinheiro, 2015). Other authors reported that the peaks at 78 °C and 126.6 °C were associated with compound dehydration, and the peaks at 192.5 °C and 205.5 °C were related to liquid–solid transition and berberine crystallization, respectively. Guo et al. (2017) and Zhang et al. (2014b) also reported berberine peaks at 100.1 °C, 192.6 °C and 288.9 °C. Considering the absence of new transition peaks in berberine nanoparticles and physical mixture, the DSC thermograms suggested physical interaction between P-407 and berberine, so that berberine-loaded nanoparticles were probably converted to an amorphous state.

The FTIR spectrum of pure berberine showed absorption bands at 3000 cm^{-1} due to aromatic vibration (C═C and C═N), the iminium (C═N+) double bond at 1603 cm^{-1} and the aromatic C═C bending vibration at 1505 cm^{-1}. Poloxamer 407 showed absorption bands at 2900 cm^{-1} (C—H stretch) and 1110 cm^{-1} (C—O stretch) (Shrimal et al., 2019). The same absorption bands were reported by other works (Battu et al., 2010; Pinheiro, 2015). The interactions for solid dispersion production possibly occurred between the Poloxamer 407 hydroxyl group (O—H) and berberine iminium group (C═N+), Sine it is possible to identify a reduction in both group's intensity when comparing the physical mixture and the nanoparticles spectra. Guo et al. (2017) described that solid dispersion interaction between berberine and Eudragit S100 occurred via intermolecular hydrogen bonding between Eudragit's C═O functions with the same group of berberine.

3.2. *In vitro cytotoxicity, anti-inflammatory and antioxidant activities*

Results of the *in vitro* toxicity against CaCo cell line, MCF-7 (breast adenocarcinoma), NCIH460 (non-small cell lung carcinoma), VERO cells, and porcine liver cells (PLP2) are presented in Table 1. Anti-inflammatory in RAW 264.7 (murine macrophages), antihaemolytic and antioxidant activities are also presented in Table 1.

Cytotoxicity was higher for free berberine than for encapsulated berberine, except for the MCF-7 cell lines, which presented similar values, and both may be considered cytotoxic for tumoral cells. Pure berberine was dispersed in DMSO because its water solubility is low (5.27 ± 0.29 mM at 25 °C (Battu et al., 2010)) meaning that the assessment of cytotoxicity in water could be compromised due to the sedimentation of the insoluble fraction of berberine during the analysis. Also, the insoluble fraction would not be available to the cells. Pure berberine exerted higher cytotoxicity on CaCo, NCI-H460 and PLP2 tumoral cell lines when compared to the nanoparticles, probably due to the fact that the presence of the encapsulant hindered the action of berberine on the cells. On the other hand, it is worth pointing out that the encapsulation allowed berberine to exert cytotoxicity on tumor cells in an aqueous medium which is important information that otherwise could be impacted by its low water solubility and low bioavailability. The same behavior was reported by Sá et al. (2019) with encapsulated curcuminoids using the same technique reported here.

Both samples presented interesting anti-inflammatory activity using the Nitric Oxide (NO) production model in RAW 264.7 cells, with berberine presenting higher activity (8.1 ± 0.1 μg.mL^{-1}) and the nanoparticles lower activity (26.7 ± 10.1 μg.mL^{-1}), when compared to the dexamethasone control (16,1 ± 1,0 μg.mL-1). RAW 264.7 cells are macrophages with the known capacity of releasing pro-inflammatory cytokines as a response to different stimulus. The released cytokines are then responsible for the production of Nitric Oxide (NO) that is involved in the immune response function. The overexpression of these

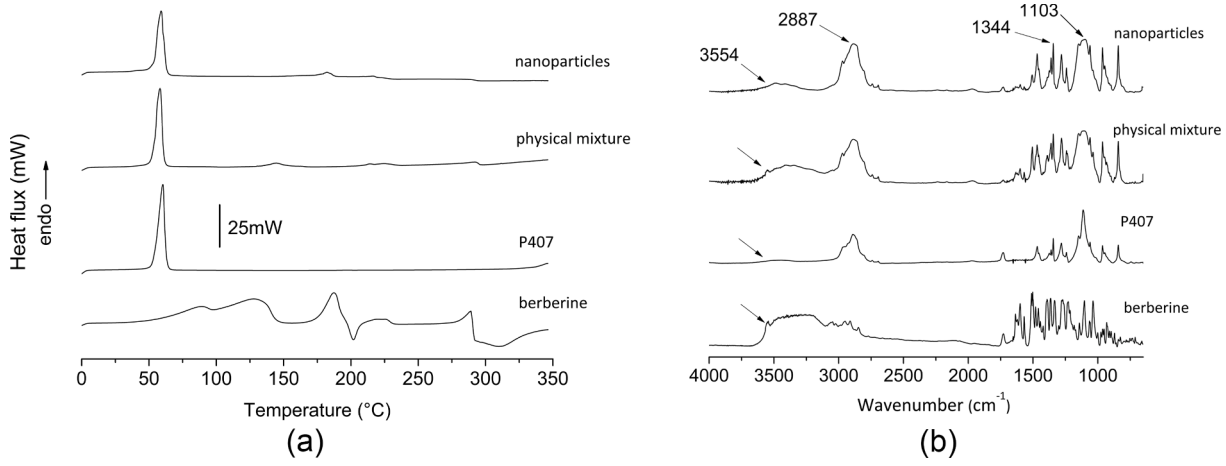

Fig. 3. (A) DSC thermograms and (B) FTIR spectra of the berberine-loaded solid dispersion with a 10:1 Poloxamer:berberine mass proportion, including data of berberine, encapsulant (Poloxamer 407) and the physical mixture between berberine and Poloxamer 407 at the same proportion.

Table 1
Cytotoxic activity against selected cell lines, anti-inflammatory activity (IC_{50} values) and antihemolytic (OxHLIA) and TBARS formation inhibition activity (IC_{50} values, $\mu g.mL^{-1}$) of berberine and the berberine-loaded solid dispersion.

	Berberine	Berberine-loaded solid dispersion
Cytotoxic activity (GI_{50} values, $\mu g.mL^{-1}$)		
CaCo	42 ± 2	252 ± 19
MCF-7	17 ± 2	20 ± 1
NCI-H460	7.1 ± 0.1	16 ± 2
PLP2	15 ± 1	49.2 ± 0.1
VERO	348 ± 30	>400
Anti-inflammatory activity (IC_{50} values, $\mu g.mL^{-1}$)		
RAW 264.7 (murine macrophages)	8.1 ± 0.1	26.7 ± 0.1
Antioxidant activity (IC_{50} values, $\mu g.mL^{-1}$)		
OxHLIA (Δt = 60 min)	27.3 ± 0.8	756 ± 40
TBARS	3.08 ± 0.09	0.76 ± 0.01

GI_{50} values ($\mu g.mL^{-1}$) for Ellipticine as cytotoxic activity control: CaCo-2 (1.21 ± 0.02), MCF-7 (1.02 ± 0.02), NCI-H460 (1.42 ± 0.0), PLP2 (1.41 ± 0.1), VERO (1.4 ± 0.1); IC_{50} values ($\mu g.mL^{-1}$) for Dexamethasone as anti-inflammatory activity control (16,1 ± 1,0); IC_{50} values ($\mu g.mL^{-1}$) for Trolox as antioxidant control: 22 ± 1 (OxHLIA Δt = 60 min); 23 ± 0.4 (TBARS).

cytokines is related to the development of several diseases, and in general, compounds with anti-inflammatory activity can inhibit cytokines expression, reducing NO production, thus diminishing the inflammatory responses and their effects (Zhao et al., 2010).

Berberine provided the highest antioxidant activity in the OxHLIA test when compared to the nanoparticles, but nanoparticles were more efficient in the TBARS test. This could be correlated to the type of radicals generated in each method since in TBARS only hydrophobic radicals are formed, while hydrophilic and hydrophobic radicals are present in the OxHLIA test (Hatia et al., 2014; Prieto & Vázquez, 2014).

All tests demonstrated that berberine may present activity in water medium after encapsulation which otherwise was only observed when a good solvent was present (DMSO in this case).

3.3. Cytotoxic and genotoxic analyses in Allium cepa L

Fig. 4 presents the mitotic index found in root meristems of *A. cepa* when exposed to berberine and the berberine-loaded solid dispersion (at 1, 3, and 10 wt%), to the encapsulant (poloxamer 407 at 10 wt%) and also to MMS (positive control at $4x10^{-4}$ mol.L^{-1}). The number of mitotic changes found in 3000 cells in root meristems of *A. cepa* when exposed to berberine and the berberine-loaded solid dispersion (at 1, 3, and 10 wt%) are presented in Table 2. Fig. 5 presents microscopy images of the meristem cells of *A. cepa* after 48 h in contact with the solutions (size bar equals to 10 μm).

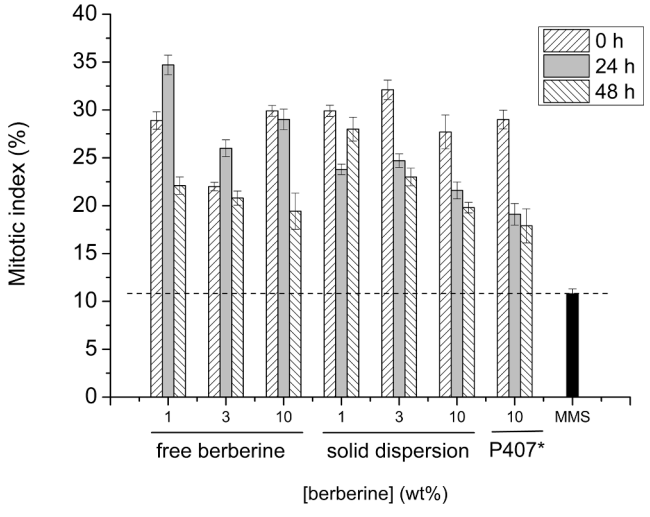

Fig. 4. Mitotic index found in root meristems of *A. cepa* when exposed to berberine and the berberine-loaded solid dispersion, to poloxamer 407 (* P407, 10 wt% poloxamer concentration), and to MMS (positive control, $4x10^{-4}$ mol.L^{-1}).

The mitotic indices observed for berberine (free or encapsulated) did not vary during the exposure time when compared to the control group (0 h). Also, the encapsulant used (Poloxamer 407) in the present study was not cytotoxic to meristematic cells from *A. cepa* roots at any exposure time. The analyzed concentrations of encapsulated berberine, encapsulant, and encapsulated berberine did not cause a significant number of cellular alterations to the meristems in any of the analyzed periods, being non-genotoxic. The *A. cepa* model was used to assess cytotoxicity and genotoxicity mostly for metallic nanoparticles of zinc (Kumari et al., 2011), cobalt (Ghodake et al., 2011), and silver (Casillas-figueroa et al., 2020; Ghodake et al., 2011). It is worth noting that in commercial polymer-based Ag nanoparticles, the presence of high amounts of the encapsulating agent was able to modulate toxic effects of silver (Casillas-figueroa et al., 2020). Also, only at high doses berberine is known to affect cell growth in A. cepa roots as demonstrated by the classic experiments of Molero et al. (1985).

3.4. Enzyme activity assays and reaction kinetics

In silico docking. To better understand the binding mechanism of berberine against AChE, docking studies were performed using Autodock Vina docking software. Only structures from *Tetronarce californica* were available for AChE and these were selected for this study (PDB: 6G1U). The predicted binding free energy value (predΔG) obtained by AutoDock Vina was equal to −8.3 kcal/mol for AChE. These predΔG value was translated into predicted *Ki* values (Pred*Ki*), and the value obtained was 877.3 nmol/L for AChE.

Along with the predicted ΔG and *Ki* values, usually termed SCORE analysis, it is also possible to analyze the predicted 3D binding conformation, usually termed POSE analysis. Fig. 6 presents the selected X-ray structure for AChE (PDB: 6G1U) along with the presentation of the berberine molecule. Also, a representation of the huprine derivative was included as pink wire lines in Fig. 6 B) because it is a known inhibitor of AChE (Galdeano et al., 2018). It is worth noting that the docking conformation of the huprine derivative superimposed very well with the co-crystallized conformation.

Table 2
Number of cellular changes in root meristems of *A. cepa* exposed to different concentrations of berberine, berberine-loaded solid dispersion, and the encapsulant (Poloxamer 407) in 0, 24, and 48 h exposure times.

		Number of Chromosomal alterations in 3000 cells		
MMS (positive control) (4×10^{-4} mol.L^{-1})		149		
	Concentration (%)	**0 h (Control group)**	**24 h**	**48 h**
Berberine	1	3	6	3
	3	3	6	3
	10	3	6	6
Berberine-loaded solid dispersion	1	3	6	3
	3	3	3	3
	10	3	6	6
Poloxamer 407	–	3	3	3

MMS: methyl methane sulfonate in 24 h. Means compared by the Scott-Knott test at 0.05 significance. In each treatment, equal letters mean that there were no difference indices of cellular changes between the evaluated exposure times (0, 24 and 48 h).

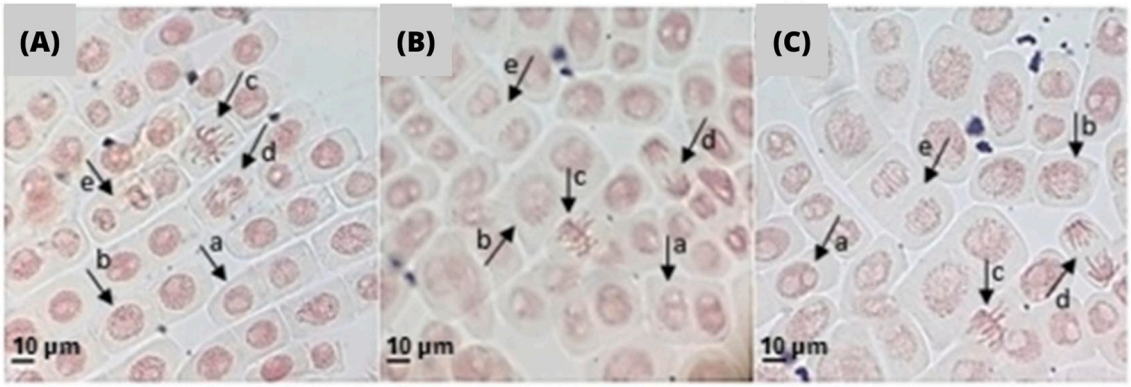

Fig. 5. Radicular meristems exposed to (A) distilled water, (B) free berberine, and (C) berberine-loaded solid dispersion. 10:1 Poloxamer:berberine mass proportion in both cases. Cells in interphase and cell division stages. The lowercase letters accompanying the arrows represent the phase of cell cycle: a- interphase; b- prophase; c- metaphase; d- anaphase; e- telophase. Size bar: 10 µm.

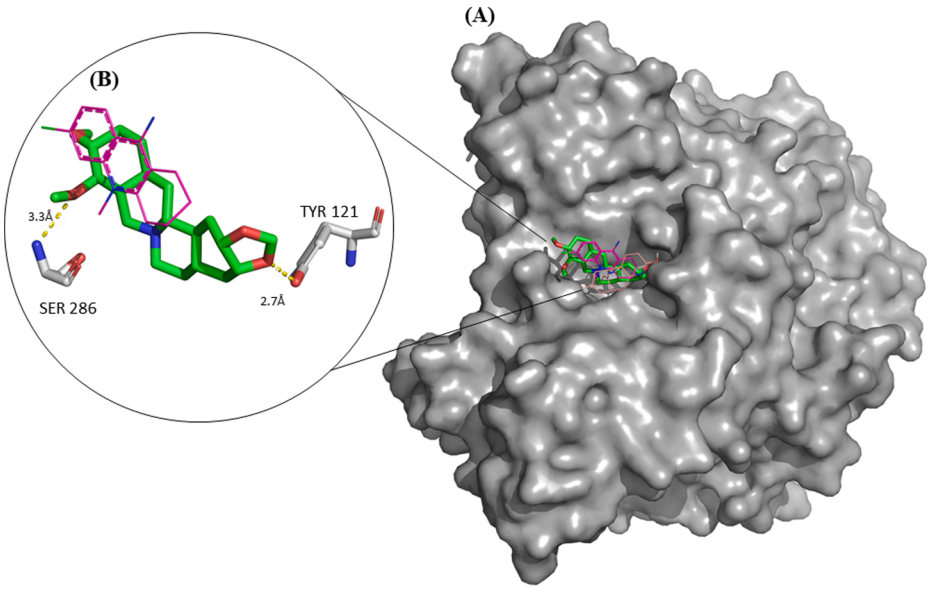

Fig. 6. Docking conformation of berberine with the AChE active site (A), and detailed interaction profile of berberine with key amino acid residues (B). Berberine is presented in green (sticks), key amino acid residues are presented in white (sticks) and the H-bonds of berberine with key amino acid residues are presented in yellow (traced lines). For reference, it is also represented the co-crystallized huprine derivative structure (pink color, wire lines in B), that is present in the X-ray AChE structure used for this docking study (PDB: 6G1U). (For interpretation of the references to color in this figure legend, the reader is referred to the web version of this article.)

When analyzing berberine docked conformation against AChE, it may be observed that two hydrogen bonds were predicted to interact with SER286 and TYR121. Overall, credible docked binding conformations of berberine were predicted against AChE by AutoDock Vina software, with satisfactory binding site pocket occupation. Honorio et al. (2021) applied docking analysis to investigate the interaction of protoberberine alkaloids against acetylcholinesterase (AChE) using molecular dynamics simulations and QM/MM calculations, and the results obtained were similar.

IC_{50} and Lineweaver-Burk reciprocal plot. Berberine and the berberine-loaded solid dispersion induced a dose-dependent inhibition in the activity of the electric eel AChE (Fig. 6A). It is worth noting that Poloxamer 407 did not present influence per se on AChE (Sá et al. 2019). Different concentrations of berberine significantly inhibited AChE *in vitro*, and the concentration that inhibited 50% of AChE activity (IC_{50}) was 0.32 ± 0.02 µmol/L. Similar AChE inhibition induced by berberine was reported in the literature (Huang et al., 2012; Jannat et al., 2019; Jung et al., 2009; Su et al., 2013). Berberine solid dispersion also significantly inhibited AChE activity but in a lower extent, with an IC_{50} value of 0.54 ± 0.06 µmol/L. Grella Miranda et al. (2020a, 2020b) evaluated the influence of free lutein and lutein-loaded nanoparticles on the AChE activity at 100, 200 and 300 µmol/L. Inhibition was only detected at 200 and 300 µmol/L and the IC_{50} value found was 265 µmol/L and 262 µmol/L for the free lutein and lutein-loaded nanoparticles. Singh et al. (2021) produced berberine-loaded lipid-coated mesoporous silica nanoparticles and found that the nanostructures presented higher AChE inhibitory activity than pure berberine in rats, however authors stated that this behavior may be explained by the improved capacity of the nanoparticles in trespassing the Blood Brain Barrier (BBB).

AChE enzyme kinetics was modified by incubation with berberine and berberine-loaded solid dispersion in the presence of five different substrate concentrations (ASCh; Fig. 7). In the Michaelis-Menten plot, concentrations between 0.1 and 3 µmol/L of berberine significantly decreased the AChE activity. Similarly, the increase in berberine solid dispersion concentration also reduced the AChE activity compared with the control (H_2O curve).

The AChE inhibition mechanism was determined by the Lineweaver-Burk reciprocal plot. Considering that the intersection of the lines occurred at the same point on the *x*-axis, the incubation with berberine and the solid dispersion inhibited AChE in a non-competitive manner. The inhibition constant *Ki* was estimated by Lineweaver-Burk reciprocal plots, Ki values for berberine and berberine-loaded solid dispersion were 252.9 ± 8.85 nmol/L and 424.2 ± 17.01 nmol/L, respectively. Other studies also reported that berberine induced the non-competitive AChE inhibition and similar *Ki* values (Huang et al., 2010; Mak et al., 2014; Su et al., 2013). It is important to notice that the experimental Ki value

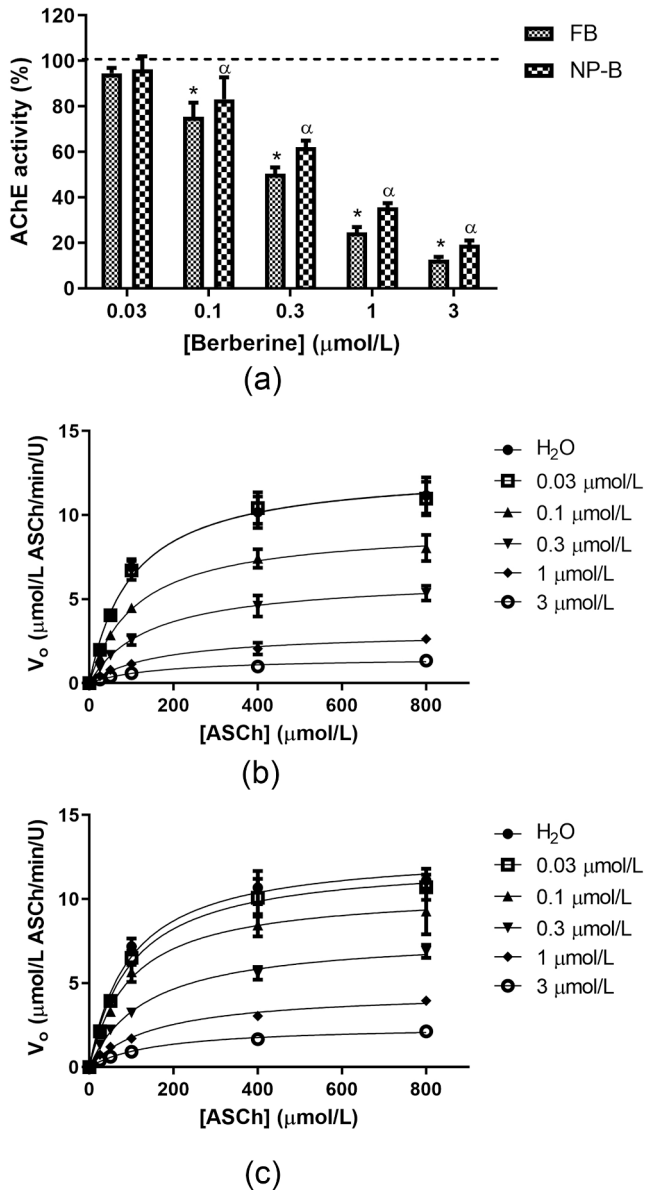

Fig. 7. *In vitro* enzyme activity of free berberine (berberine) and the berberine-loaded solid dispersion (berberine-loaded solid dispersion). 10:1 Poloxamer: berberine mass proportion in both cases. (A) AChE was incubated with different concentrations (0.03–3 μmol/L) of berberine or berberine-loaded solid dispersion; the substrate was acetylthiocholine iodide (ASCh; 800 μmol/L); (B) Michaelis-Menten plots of berberine (berberine) and (C) berberine-loaded solid dispersion (berberine-loaded solid dispersion).

obtained for berberine against AChE (252.9 ± 8.85 nmol/L) is in the same order of magnitude as the predicted Ki value (877.3 nmol/L), obtained using molecular docking, thus validating the docking results presented above.

Non-linear parameter estimation. The particle swarm optimization (PSO) algorithm is a heuristic optimization method, based on empirical evolutionary rules that frequently mimic successful optimization strategies found in nature (Schwaab et al., 2008). PSO algorithm is initialized with a population of random solutions, called particles. Each particle is associated with a corresponding velocity which determines the direction and distance of its flight, like birds towards their prey. Each particle follows the optimal particle to fly through the search space at the corresponding velocity, and the velocities are updated according to their historical behaviors at each flight until the optimal solution is found. Finally, the Gauss-Newton method employs the initial value calculated by the PSO algorithm, which improves the computational efficiency and accuracy of the algorithm(Li & Zhong, 2019).

The likelihood confidence region obtained with the PSO for the Michaelis Menten Equation is shown in Fig. 8A. It is possible to observe that the likelihood confidence region presents an elliptical form, indicating that the points used by the PSO during the minimization can be used effectively for the definition of the parameter confidence region (Schwaab et al., 2008).

In Fig. 8 it is possible to verify the agreement between experimental and predicted data. The predicted values found under these conditions for km and Vmax are presented in Table 3 and the experimental validation is presented in Fig. 9. Wetwitayaklung et al. (2007) also evaluated the kinetics parameters of the catalyzed reaction of acetylthiocholine iodide (ASCh) hydrolysis into thiocholine and acetic acid by electric eel acetylcholinesterase type III (AChE), however, the Lineweaver-Burk plot was used for that. The authors determined values of km and Vmax equal to 32 μmol/L and 0.017 μmol/L ASCh/min/μg, respectively. In another work, López et al. (2015) determined a km equal to 0.52 ± 0.02 mmol/L, also using the Lineweaver-Burk plot. Possibly, these differences can be attributed to different proportions of the reagents during the assay, such as enzyme concentration (0.09 U/mL in the present work and 5 U/mL used by López et al.(2015)) although the method used was the same (Ellman et al., 1961).

A model discrimination strategy was applied to verify the inhibition mechanism associated with pure berberine and nanoencapsulated berberine against AChE. Thus, the hybrid strategy was applied using Equations (10), (11), (12), and (13), as well as the previously determined km and Vmax in the absence of inhibitors. Results obtained for each case are presented in Table 3, where it is possible to observe that the kinetic data were not explained by the Competitive, Uncompetitive, and Non-competitive pure models, for both inhibitors (pure and nanoencapsulated berberine). This result is clear by the analysis of the CHI^2 interval and the objective function determined (Fobj). Although the Fobj determined for the data when applied to the Non-competitive mixed model still surpasses slightly the upper CHI^2 limit, the confidence regions between the model's parameters present an elliptical shape, as can be observed for pure berberine in Fig. 10 and nanoencapsulated berberine in Fig. 11.

The average value of the estimated K_{ic} for AChE non-competitive mixed inhibition by berberine (Table 3) is below the result found by the Lineweaver-Burk reciprocal plots (K_i = 252.9 nmol/L). However, Lineweaver-Burk determined K_i value is between the confidence interval determined for K_{ic}. The K_{iu} value estimated by the PSO is above Lineweaver-Burk K_i, but it is also located in the K_{iu} confidence interval. Although K_{iu} and K_{ic} confidence intervals are not completely overlapped, there is a common region between them, in which Lineweaver-Burk K_i can be found. In the case of the pred*Ki* determined with the molecular docking for AChE inhibition by pure berberine, the result found (877.3 nM) is in the same order of magnitude as the values obtained with the Lineweaver-Burk and PSO methods. Due to the inherent limitations of molecular docking, the predicted and experimental values are not always comparable. The fact that similar results were obtained suggests that molecular docking, using AutoDock Vina (Eberhardt et al., 2021), is able to predict the inhibition order of magnitude of berberine against AChE.

Regarding nanoencapsulated berberine action to inhibit AChE, the PSO estimated K_{ic} was the same found for pure berberine. However, the estimated K_{iu} value was 4-fold higher than the result determined for free berberine. Furthermore, for both inhibitors (pure and nanoencapsulated berberine) $K_{iu} > K_{ic}$, a result that indicates predominantly competitive inhibition (CORTÉS et al., 2001). Competitive inhibition occurs when inhibitors bind to the initial free enzyme form in a manner that blocks the binding of substrate molecules. On the other hand, uncompetitive inhibition occurs when the inhibitor binds to substrate-bound forms of the enzyme (preferentially or even exclusively). In this case, the binding

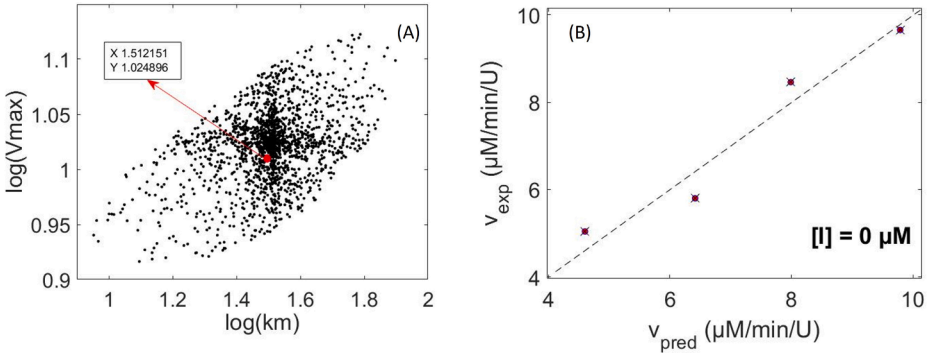

Fig. 8. (A) Likelihood confidence region and optimal point (red point) obtained through Particle Swarm Optimization for AChE catalyzed reaction (no inhibitor added, [I] = 0 µmol/L); (B) Experimental results and model prediction of the initial rate (v at 0.2 min) of the AChE catalyzed reaction for the five substrate concentrations evaluated ([ASCh] = 25, 50, 100, 400, 800 µmol/L). (For interpretation of the references to color in this figure legend, the reader is referred to the web version of this article.)

Table 3
Parameters estimated and objective function values for no inhibitor added, pure berberine, and nanoencapsulated berberine as inhibitors.

Model	Inhibitor	CHI^2_{inf}	CHI^2_{sup}	Fobj	Estimated parameters
Michaelis Menten	–	0.216	9.348	0.804	**km (nmol/L)** 8970 ≤ 32520 ≤ 79030 **Vmax (nM ASCh/min/U)** 8250 ≤ 10590 ≤ 13260
Competitive inhibition	**Pure berberine**	11.689	38.076	495.425	–
	Nano berberine	11.689	38.076	217.032	–
Uncompetitive inhibition	**Pure berberine**	10.982	36.781	131.819	–
	Nano berberine	10.982	36.781	72.349	–
Non-competitive Mixed inhibition	**Pure berberine**	10.982	36.781	79.712	**K_{ic} (nmol/L)** 100 ≤ 190 ≤ 450 **K_{iu} (nmol/L)** 220 ≤ 460 ≤ 1100 **a (dimensionless)** 0.67 ≤ 0.92 ≤ 1.20
	Nano berberine	10.982	36.781	41.907	**K_{ic} (nmol/L)** 100 ≤ 190 ≤ 430 **K_{iu} (nmol/L)** 420 ≤ 760 ≤ 1730 **a (dimensionless)** 0.78 ≤ 0.96 ≤ 1.17
Non-competitive Pure inhibition	**Pure berberine**	11.689	38.076	92.459	–
	Nano berberine	11.689	38.076	62.591	–

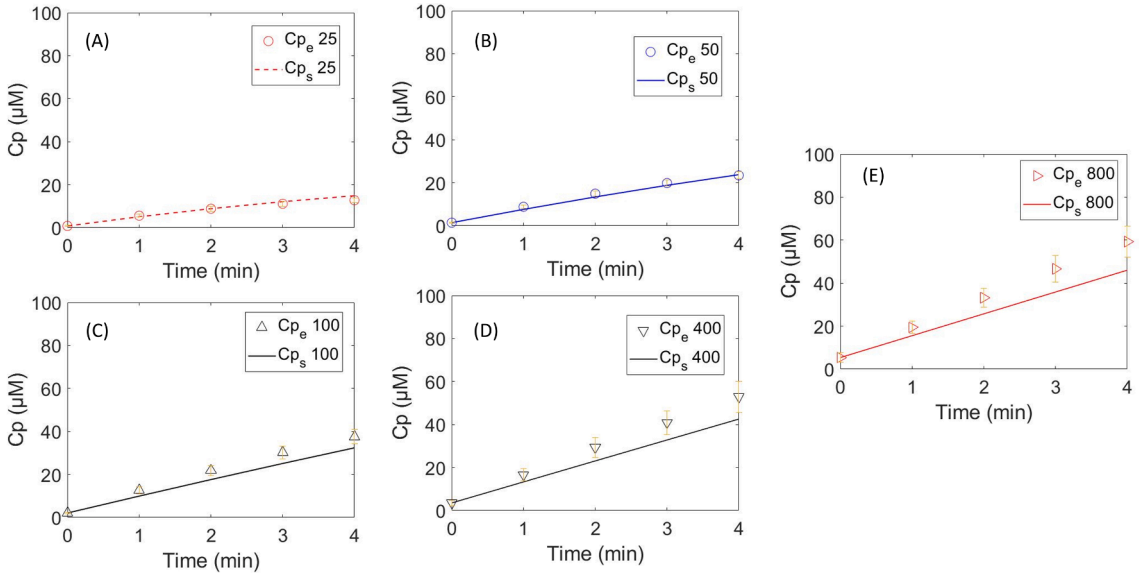

Fig. 9. Thiocholine production during the kinetic analysis (Cp, µM) with no inhibitor added ([I] = 0 µM) for different substrate concentrations (A) [ASCh] = 25 µM; (B) [ASCh] = 50 µM, (C) [ASCh] = 100 µM, (D) [ASCh] = 400 µM, (E) [ASCh] = 800 µM. Cp_e: experimental results; Cp_s: simulation results using km and Vmax estimated through non-linear estimation procedure.

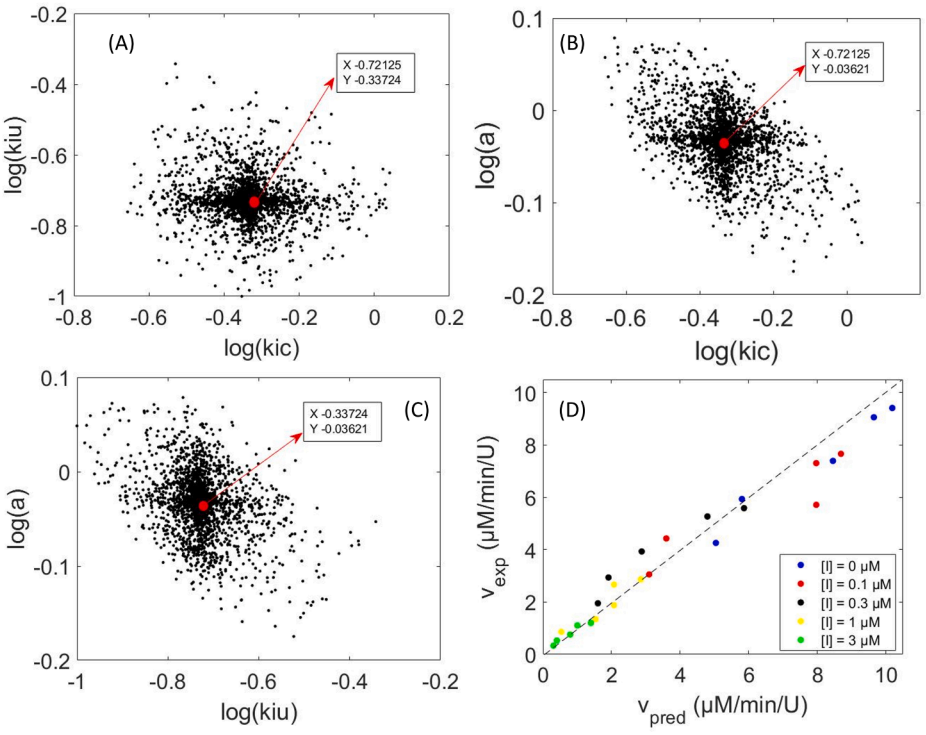

Fig. 10. Likelihood confidence regions and optimal points (red points) obtained through Particle Swarm Optimization for the data AChE catalyzed reaction with pure berberine as inhibitor added, applied in Noncompetitive Mixed model: (A) $\log(K_{iu}) \times \log(K_{ic})$, (B) $\log(a) \times \log(K_{ic})$, (C) $\log(a) \times \log(K_{iu})$. (D) Experimental results and model prediction of the initial rate (v at 0.2 min) of the AChE catalyzed reaction for pure berberine as inhibitor ([I] = 0, 0.1, 0.3, 1 and 3 μmol/L). (For interpretation of the references to color in this figure legend, the reader is referred to the web version of this article.)

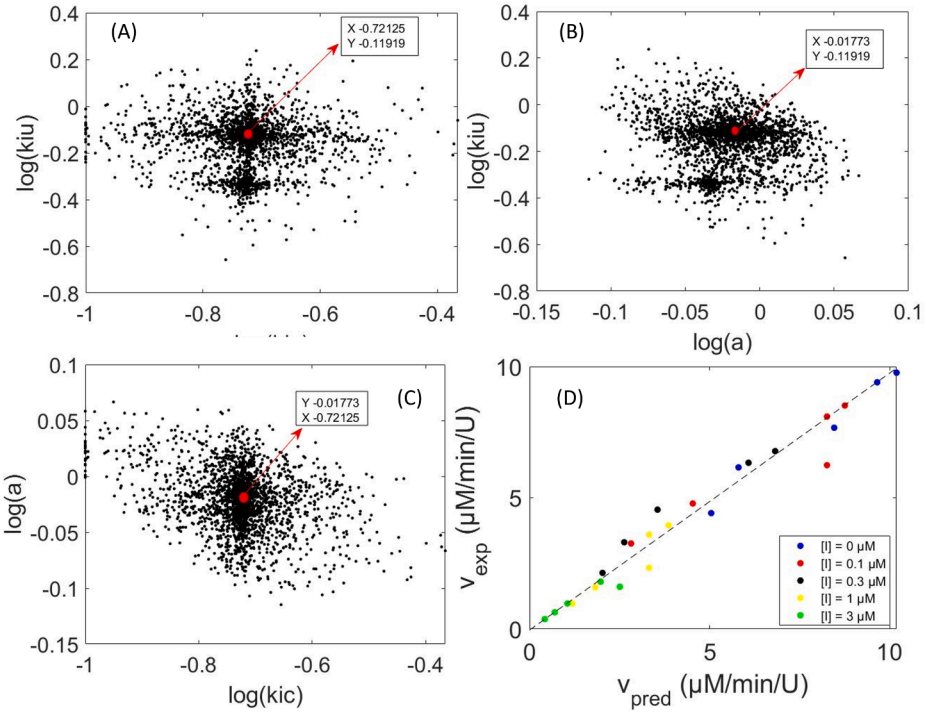

Fig. 11. Likelihood confidence regions and optimal points (red points) obtained through Particle Swarm Optimization for the data AChE catalyzed reaction with nanoencapsulated berberine as inhibitor added, applied in Noncompetitive Mixed model: (A) $\log(K_{iu}) \times \log(K_{ic})$, (B) $\log(a) \times \log(K_{ic})$, (C) $\log(a) \times \log(K_{iu})$. (D) Experimental results and model prediction of the initial rate (v at 0.2 min) of the AChE catalyzed reaction for nanoencapsulated berberine as inhibitor ([I] = 0, 0.1, 0.3, 1 and 3 μmol/L). (For interpretation of the references to color in this figure legend, the reader is referred to the web version of this article.)

affinities for the inhibitor and the substrate are mutually synergistic. The mixed non-competitive inhibition mechanism includes all the possibilities mentioned above (Copeland et al., 2007). Thus, in the case of free and encapsulated berberine inhibition, the main action is the attack on the binding site, impairing substrate linkage.

4. Conclusions

A polymeric solid dispersion containing berberine was evaluated as an inhibitor of the acetylcholinesterase enzyme. This extensive study included *in silico* simulation, kinetic modeling, and *in vitro* kinetic studies. Spectroscopic and thermal analyses showed satisfactory interaction between the encapsulant (Poloxamer 407) and berberine, and transmission electron microscopy showed the formation of nanometric

particles when the system was redispersed in water. Taking into consideration the inherent advantages and limitations of the methods used here, *in vitro*, *in silico* and kinetic modeling pointed in the direction that the action of free and solid dispersion berberine is explained by a non-competitive mixed model. No genotoxicity and cytotoxicity were detected in the *in vivo* assays in *Allium cepa*. Also, berberine in the solid dispersion exerted an improved cytotoxic effect on tumoral cells even in water, despite the low water solubility of berberine.

CRediT authorship contribution statement

Fernanda Vitória Leimann: Conceptualization, Writing – original draft, Software. **Luma Borges de Souza:** Investigation, Formal analysis. **Byanca Pereira Moreira de Oliveira:** Investigation, Writing – original draft. **Bruna Franzon Rossi:** Investigation, Formal analysis. **Patrícia Sabino da Silva:** Investigation, Writing – original draft. **Carlos Seiti Hurtado Shiraishi:** Software, Investigation. **Vanessa Kaplum:** Investigation, Writing – original draft. **Rui Miguel Abreu:** Software, Formal analysis. **Carla Pereira:** Investigation, Writing – original draft. **Lillian Barros:** Resources, Methodology, Supervision. **Ana Paula Peron:** Resources, Methodology. **Rafael Porto Ineu:** Resources, Writing – review & editing. **Bruno Francisco Oechsler:** Formal analysis, Writing – review & editing. **Claudia Sayer:** Formal analysis, Project administration, Funding acquisition. **Pedro Henrique Hermes de Araújo:** Formal analysis, Supervision. **Odinei Hess Gonçalves:** Resources, Project administration, Funding acquisition.

Declaration of Competing Interest

The authors declare that they have no known competing financial interests or personal relationships that could have appeared to influence the work reported in this paper.

Data availability

Data will be made available on request.

Acknowledgements

The authors are grateful to CNPq and CAPES (Finance Code 001) for the support. The authors are grateful to the Foundation for Science and Technology (FCT, Portugal) for financial support through national funds FCT/MCTES to CIMO (UIDB/00690/2020). The authors are also grateful to FCT for financial support through national funds FCT/MCTES (PIDDAC) to CIMO (UIDB/00690/2020 and UIDP/00690/2020) and SusTEC (LA/P/0007/2020). L. Barros and C. Pereira thank FCT, P.I., for the contracts through the institutional scientific employment program-contract.

Data availability statement

The datasets generated during and/or analyzed during the current study are available from the corresponding author on reasonable request.

References

Abd El-Wahab, A. E., Ghareeb, D. A., Sarhan, E. E. M., Abu-Serie, M. M., & El Demellawy, M. A. (2013). In vitro biological assessment of berberis vulgaris and its active constituent, berberine: Antioxidants, anti-acetylcholinesterase, anti-diabetic and anticancer effects. *BMC Complementary and Alternative Medicine, 13*. https://doi.org/10.1186/1472-6882-13-218

Abreu, R. M. V., Ferreira, I. C. F. R., Calhelha, R. C., Lima, R. T., Vasconcelos, M. H., Adega, F., … Queiroz, M. J. R. P. (2011). Anti-hepatocellular carcinoma activity using human HepG2 cells and hepatotoxicity of 6-substituted methyl 3-aminothieno [3,2-b]pyridine-2- carboxylate derivatives: In vitro evaluation, cell cycle analysis and QSAR studies. *European Journal of Medicinal Chemistry, 46*(12), 5800–5806. https://doi.org/10.1016/j.ejmech.2011.09.029

Ahmed, B., Dwivedi, S., Abdin, M. Z., Azam, A., Al-Shaeri, M., Khan, M. S., … Musarrat, J. (2017). Mitochondrial and Chromosomal Damage Induced by Oxidative Stress in Zn2+ Ions, ZnO-Bulk and ZnO-NPs treated Allium cepa roots. *Scientific Reports, 7*. https://doi.org/10.1038/srep40685

Aledo, J. C., & Juan Aledo, C. C. (2021). *Enzyme kinetic parameters estimation: A tricky task? double-reciprocal*. https://doi.org/10.1002/bmb.21522.

Almeida, M., Rocha, B. A., Francisco, C. R. L., Miranda, C. G., Santos, P. D. de F., Araújo, P., Sayer, C., Leimann, F. v, Gonçalves, O. H., & Bersani-Amado, C. C. A. (2018). Evaluation of the in vivo acute antiinflammatory response of curcumin-loaded nanoparticles. *Food & Function, 9*, 440–449. https://doi.org/10.1039/C7FO01616F.

Battu, S. K., Repka, M. A., Maddineni, S., Chittiboyina, A. G., Avery, M. A., & Majumdar, S. (2010). Physicochemical Characterization of Berberine Chloride: A Perspective in the Development of a Solution Dosage Form for Oral Delivery. *AAPS PharmSciTech, 11*(3), 1466–1475. https://doi.org/10.1208/s12249-010-9520-y

Bikiaris, D. N., Papageorgiou, G. Z., Papadimitriou, S. A., Karavas, E., & Avgoustakis, K. (2009). Novel Biodegradable Polyester Poly(Propylene Succinate): Synthesis and Application in the Preparation of Solid Dispersions and Nanoparticles of a Water-Soluble Drug. *AAPS PharmSciTech, 10*(1), 138–146. https://doi.org/10.1208/s12249-008-9184-z

Bisswanger, H. (2008). *Enzyme kinetics : Principles and methods*. Wiley-VCH.

Bonciu, E., Firbas, P., Fontanetti, C. S., Wusheng, J., Karaismailoğlu, M. C., Liu, D., Menicucci, F., Pesnya, D. S., Popescu, A., Romanovsky, A. v., Schiff, S., Ślusarczyk, J., de Souza, C. P., Srivastava, A., Sutan, A., & Papini, A. (2018a). An evaluation for the standardization of the Allium cepa test as cytotoxicity and genotoxicity assay. *Caryologia, 71*(3), 191–209. https://doi.org/10.1080/00087114.2018.1503496.

Butt, A. M., Iqbal, M. C., Amin, M., & Katas, H. (2015). Synergistic effect of pH-responsive folate-functionalized poloxamer 407-TPGS-mixed micelles on targeted delivery of anticancer drugs. *International Journal of Nanomedicine, 10*, 1321–1334. https://doi.org/10.2147/IJN.S78438

Cai, Z., Wang, C., & Yang, W. (2016). Role of berberine in Alzheimer’s disease. *Neuropsychiatric Disease and Treatment, 12*, 2509–2520. https://doi.org/10.2147/NDT.S114846

Casillas-figueroa, F., Arellano-garcía, M. E., Leyva-aguilera, C., Ruíz-ruíz, B., Vázquez-gómez, R. L., Radilla-chávez, P., Chávez-santoscoy, R. A., Pestryakov, A., Toledano-magaña, Y., García-ramos, J. C., & Bogdanchikova, N. (2020). Argovit™ silver nanoparticles effects on allium cepa: Plant growth promotion without cyto genotoxic damage. *Nanomaterials, 10*(7), 1–20. https://doi.org/10.3390/nano10071386

Chenthamara, D., Subramaniam, S., Ramakrishnan, S. G., Krishnaswamy, S., Essa, M. M., Lin, F.-H., & Qoronfleh, M. W. (2019). Therapeutic efficacy of nanoparticles and routes of administration. *Biomaterials Research, 23*(1), 20. https://doi.org/10.1186/s40824-019-0166-x

Copeland, R. A., Harpel, M. R., & Tummino, P. J. (2007). Targeting enzyme inhibitors in drug discovery. *Expert Opinion on Therapeutic Targets, 11*(7), 967–978. https://doi.org/10.1517/14728222.11.7.967

Cortés, A., Cascante, M., Cárdenas, M. L., & Cornish-Bowden, A. (2001). Relationships between inhibition constants, inhibitor concentrations for 50% inhibition and types of inhibition: New ways of analysing data. *Biochemical Journal, 357*(1), 263–268. https://doi.org/10.1042/bj3570263

Creasy, A., Barker, G., Yao, Y., & Carta, G. (2015). Systematic interpolation method predicts protein chromatographic elution from batch isotherm data without a detailed mechanistic isotherm model. *Biotechnology Journal, 10*(9), 1400–1411. https://doi.org/10.1002/BIOT.201500089

Desai, S., Poddar, A., & Sawant, K. (2016). Formulation of cyclodextrin inclusion complex-based orally disintegrating tablet of eslicarbazepine acetate for improved oral bioavailability. *Materials Science and Engineering: C, 58*, 826–834. https://doi.org/10.1016/j.msec.2015.09.019

Dumortier, G., Grossiord, J. L., Agnely, F., & Chaumeil, J. C. (2006). A review of poloxamer 407 pharmaceutical and pharmacological characteristics. In *Pharmaceutical Research* (Vol. 23, Issue 12, pp. 2709–2728). Springer Science and Business Media Deutschland GmbH. https://doi.org/10.1007/s11095-006-9104-4.

Eberhardt, J., Santos-Martins, D., Tillack, A. F., & Forli, S. (2021). AutoDock Vina 1.2.0: New Docking Methods, Expanded Force Field, and Python Bindings. *Journal of Chemical Information and Modeling, 61*(8), 3891–3898. https://doi.org/10.1021/acs.jcim.1c00203

Ellman, G. L., Courtney, K. D., Andres, V., & Featherstone, R. M. (1961). A new and rapid colorimetric determination of acetylcholinesterase activity. *Biochemical Pharmacology, 7*(2), 88–95. https://doi.org/10.1016/0006-2952(61)90145-9

Evans, B. C., Nelson, C. E., Yu, S. S., Beavers, K. R., Kim, A. J., Li, H., … Duvall, C. L. (2013). Ex Vivo Red Blood Cell Hemolysis Assay for the Evaluation of pH-responsive Endosomolytic Agents for Cytosolic Delivery of Biomacromolecular Drugs. *Journal of Visualized Experiments, 73*, 1–5. https://doi.org/10.3791/50166

Fan, D., Liu, L., Wu, Z., & Cao, M. (2019). Combating Neurodegenerative Diseases with the Plant Alkaloid Berberine: Molecular Mechanisms and Therapeutic Potential. *Current Neuropharmacology, 17*(6), 563–579. https://doi.org/10.2174/1570159X16666180419141613

Fiskesjo, G. (1985). The Allium test as a standard in environmental monitoring. *Hereditas, 102*, 99–100.

Freitas, P. D., Santos, D., Rafael, C., Francisco, L., Coqueiro, A., Leimann, F. V., Pinela, J., Calhelha, R. C., Porto Ineu, R., Ferreira, I. C. F. R., Bona, E., & Hess Gonçalves, O. (2019). The nanoencapsulation of curcuminoids extracted from Curcuma longa L. and an evaluation of their cytotoxic, enzymatic, antioxidant and anti-inflammatory activities †. *Food and Function, 10*, 573–582. https://doi.org/10.1039/c8fo02431f

Galdeano, C., Coquelle, N., Cieslikiewicz-Bouet, M., Bartolini, M., Pérez, B., Victòria Clos, M., Silman, I., Jean, L., Colletier, J. P., Renard, P. Y., & oz-Torrero, D. M. (2018). Increasing polarity in tacrine and huprine derivatives: Potent

anticholinesterase agents for the treatment of myasthenia gravis. *Molecules, 23*(3). https://doi.org/10.3390/molecules23030634

Gao, Y., Wang, F., Song, Y., & Liu, H. (2020). The status of and trends in the pharmacology of berberine: A bibliometric review [1985–2018]. *Chinese Medicine, 15*(1), 7. https://doi.org/10.1186/s13020-020-0288-z

Ghodake, G., Seo, Y. D., & Lee, D. S. (2011). Hazardous phytotoxic nature of cobalt and zinc oxide nanoparticles assessed using Allium cepa. *Journal of Hazardous Materials, 186*(1), 952–955. https://doi.org/10.1016/j.jhazmat.2010.11.018

Grella Miranda, C., dos Santos, P. D. F., do Prado Silva, J. T., Vitória Leimann, F., Ferreira Borges, B., Miguel Abreu, R., Porto Ineu, R., & Hess Gonçalves, O. (2020a). Influence of nanoencapsulated lutein on acetylcholinesterase activity: In vitro determination, kinetic parameters, and in silico docking simulations. *Food Chemistry*, *307*(March 2019), 125523. https://doi.org/10.1016/j.foodchem.2019.125523.

Grella Miranda, C., dos Santos, P. D. F., do Prado Silva, J. T., Vitória Leimann, F., Ferreira Borges, B., Miguel Abreu, R., Porto Ineu, R., & Hess Gonçalves, O. (2020b). Influence of nanoencapsulated lutein on acetylcholinesterase activity: In vitro determination, kinetic parameters, and in silico docking simulations. *Food Chemistry*, *307*. https://doi.org/10.1016/j.foodchem.2019.125523.

Guo, S., Wang, G., Wu, T., Bai, F., Xu, J., & Zhang, X. (2017). Solid dispersion of berberine hydrochloride and Eudragit ® S100: Formulation, physicochemical characterization and cytotoxicity evaluation. *Journal of Drug Delivery Science and Technology, 40*, 21–27. https://doi.org/10.1016/j.jddst.2017.02.003

Hatia, S., Septembre-Malaterre, A., Le Sage, F., Badiou-Bénéteau, A., Baret, P., Payet, B., Lefebvre d'hellencourt, C., & Gonthier, M. P. (2014). Evaluation of antioxidant properties of major dietary polyphenols and their protective effect on 3T3-L1 preadipocytes and red blood cells exposed to oxidative stress. *Free Radical Research, 48*(4), 387–401. https://doi.org/10.3109/10715762.2013.879985.

Herrero, O., Pérez Martín, J. M., Fernández Freire, P., Carvajal López, L., Peropadre, A., & Hazen, M. J. (2012). Toxicological evaluation of three contaminants of emerging concern by use of the Allium cepa test. *Mutation Research - Genetic Toxicology and Environmental Mutagenesis, 743*(1–2), 20–24. https://doi.org/10.1016/j.mrgentox.2011.12.028

Honorio, P., Sainimnuan, S., Hannongbua, S., & Saparpakorn, P. (2021). Binding interaction of protoberberine alkaloids against acetylcholinesterase (AChE) using molecular dynamics simulations and QM/MM calculations. *Chemico-Biological Interactions, 344*. https://doi.org/10.1016/j.cbi.2021.109523

Huang, L., Shi, A., He, F., & Li, X. (2010). Synthesis, biological evaluation, and molecular modeling of berberine derivatives as potent acetylcholinesterase inhibitors. *Bioorganic & Medicinal Chemistry, 18*(3), 1244–1251. https://doi.org/10.1016/j.bmc.2009.12.035

Huang, L., Su, T., Shan, W., Luo, Z., Sun, Y., He, F., & Li, X. (2012). Inhibition of cholinesterase activity and amyloid aggregation by berberine-phenyl-benzoheterocyclic and tacrine-phenyl-benzoheterocyclic hybrids. *Bioorganic & Medicinal Chemistry, 20*(9), 3038–3048. https://doi.org/10.1016/j.bmc.2012.02.059

Huang, Y., & Dai, W.-G. (2014). Fundamental aspects of solid dispersion technology for poorly soluble drugs. *Acta Pharmaceutica Sinica B, 4*(1), 18–25. https://doi.org/10.1016/j.apsb.2013.11.001

Imenshahidi, M., & Hosseinzadeh, H. (2019). Berberine and barberry (Berberis vulgaris): A clinical review. *Phytotherapy Research, 33*(3), 504–523. https://doi.org/10.1002/ptr.6252

Jannat, S., Balupuri, A., Ali, M. Y., Hong, S. S., Choi, C. W., Choi, Y.-H., Ku, J.-M., Kim, W. J., Leem, J. Y., Kim, J. E., Shrestha, A. C., Ham, H. N., Lee, K.-H., Kim, D. M., Kang, N. S., & Park, G. H. (2019). Inhibition of β-site amyloid precursor protein cleaving enzyme 1 and cholinesterases by pterosins via a specific structure–activity relationship with a strong BBB permeability. *Experimental & Molecular Medicine, 51*(2), 1–18. https://doi.org/10.1038/s12276-019-0205-7

Jaskirat, S., Manpreet, W., & L, H. S. (2011). SOLUBILITY ENHANCEMENT BY SOLID DISPERSION METHOD: A REVIEW. *Journal of Drug Delivery & Therapeutics*, *2013*(3), 148–155. http://jddtonline.info.

Ji, H. F., & Shen, L. (2011). Berberine: A potential multipotent natural product to combat Alzheimer's disease. In *Molecules* (Vol. 16, Issue 8, pp. 6732–6740). https://doi.org/10.3390/molecules16086732.

Joseph, A., Simo, G. M., Gao, T., Alhindi, N., Xu, N., Graham, D. J., … Nance, E. (2021). Surfactants influence polymer nanoparticle fate within the brain. *Biomaterials, 277*. https://doi.org/10.1016/j.biomaterials.2021.121086

Jung, H. A., Min, B.-S., Yokozawa, T., Lee, J.-H., Kim, Y. S., & Choi, J. S. (2009). Anti-Alzheimer and Antioxidant Activities of Coptidis Rhizoma Alkaloids. *Biological and Pharmaceutical Bulletin, 32*(8), 1433–1438. https://doi.org/10.1248/bpb.32.1433

Karavas, E., Ktistis, G., Xenakis, A., & Georgarakis, E. (2006). Effect of hydrogen bonding interactions on the release mechanism of felodipine from nanodispersions with polyvinylpyrrolidone. *European Journal of Pharmaceutics and Biopharmaceutics, 63*(2), 103–114. https://doi.org/10.1016/j.ejpb.2006.01.016

Koly, H. K., Sutradhar, K., & Rahman, M. S. (2023). Acetylcholinesterase inhibition of Alzheimer's disease: Identification of potential phytochemicals and designing more effective derivatives to manage disease condition. *Journal of Biomolecular Structure and Dynamics*. https://doi.org/10.1080/07391102.2023.2166992

Kreuter, J. (1996). Nanoparticles and microparticles for drug and vaccine delivery. In *J. Anat.*

Kulkarni, S. A., & Feng, S. S. (2011). Effects of surface modification on delivery efficiency of biodegradable nanoparticles across the blood-brain barrier. *Nanomedicine, 6*(2), 377–394. https://doi.org/10.2217/nnm.10.131

Kumari, M., Khan, S. S., Pakrashi, S., Mukherjee, A., & Chandrasekaran, N. (2011). Cytogenetic and genotoxic effects of zinc oxide nanoparticles on root cells of Allium cepa. *Journal of Hazardous Materials, 190*(1–3), 613–621. https://doi.org/10.1016/j.jhazmat.2011.03.095

Li, W., & Zhong, K. (2019). Application of improved particle swarm optimization algorithm in solving camera extrinsic parameters. *Journal of Modern Optics, 66*(18). https://doi.org/10.1080/09500340.2019.1682203

Lin, X., & Zhang, N. (2018). Berberine: Pathways to protect neurons. *Phytotherapy Research, 32*(8), 1501–1510. https://doi.org/10.1002/ptr.6107

Liu, D., Meng, X., Wu, D., Qiu, Z., & Luo, H. (2019). A Natural Isoquinoline Alkaloid With Antitumor Activity: Studies of the Biological Activities of Berberine. *Frontiers in Pharmacology, 10*(FEB), 1–12. https://doi.org/10.3389/fphar.2019.00009

Liu, P.-P., Xie, Y., Meng, X.-Y., & Kang, J.-S. (2019). History and progress of hypotheses and clinical trials for Alzheimer's disease. *Signal Transduction and Targeted Therapy, 4*(1), 29. https://doi.org/10.1038/s41392-019-0063-8

Long, J. M., & Holtzman, D. M. (2019). Alzheimer Disease: An Update on Pathobiology and Treatment Strategies. *Cell, 179*(2), 312–339. https://doi.org/10.1016/j.cell.2019.09.001

López, M. D., Campoy, F. J., Pascual-Villalobos, M. J., Muñoz-Delgado, E., & Vidal, C. J. (2015). Acetylcholinesterase activity of electric eel is increased or decreased by selected monoterpenoids and phenylpropanoids in a concentration-dependent manner. *Chemico-Biological Interactions, 229*, 36–43. https://doi.org/10.1016/J.CBI.2015.01.006

Ma, X., Zhou, J., Zhang, C. X., Li, X. Y., Li, N., Ju, R. J., … Lu, W. L. (2013). Modulation of drug-resistant membrane and apoptosis proteins of breast cancer stem cells by targeting berberine liposomes. *Biomaterials, 34*(18), 4452–4465. https://doi.org/10.1016/j.biomaterials.2013.02.066

Majidzadeh, H., Araj-Khodaei, M., Ghaffari, M., Torbati, M., Ezzati Nazhad Dolatabadi, J., & Hamblin, M. R. (2020). Nano-based delivery systems for berberine: A modern anti-cancer herbal medicine. *Colloids and Surfaces B: Biointerfaces, 194*(May), Article 111188. https://doi.org/10.1016/j.colsurfb.2020.111188

Mak, S., Luk, W. W. K., Cui, W., Hu, S., Tsim, K. W. K., & Han, Y. (2014). Synergistic Inhibition on Acetylcholinesterase by the Combination of Berberine and Palmatine Originally Isolated from Chinese Medicinal Herbs. *Journal of Molecular Neuroscience, 53*(3), 511–516. https://doi.org/10.1007/s12031-014-0288-5

Mirhadi, E., Rezaee, M., & Malaekeh-Nikouei, B. (2018). Nano strategies for berberine delivery, a natural alkaloid of Berberis. *Biomedicine & Pharmacotherapy, 104*(May), 465–473. https://doi.org/10.1016/j.biopha.2018.05.067

Molero, M. L., Hazen, M. J., & Stockert, J. C. (1985). Photodynamic Effect of Berberine Sulfate on the Growth Rate of Allium cepa Roots. *Journal of Plant Physiology, 120*(1), 91–94. https://doi.org/10.1016/S0176-1617(85)80126-7

Pandey, H., Kumar, V., & Roy, B. K. (2014). Assessment of genotoxicity of some common food preservatives using Allium cepa L. as a test plant. *Toxicology Reports, 1*, 300–308. https://doi.org/10.1016/j.toxrep.2014.06.002

Pereira, M. E., Adams, A. I. H., & Silva, N. S. (2004). 2,5-Hexanedione inhibits rat brain acetylcholinesterase activity in vitro. *Toxicology Letters, 146*(3), 269–274. https://doi.org/10.1016/j.toxlet.2003.10.009

Pinela, J., Barros, L., Carvalho, A. M., & Ferreira, I. C. F. R. (2012). Nutritional composition and antioxidant activity of four tomato (Lycopersicon esculentum L.) farmer' varieties in Northeastern Portugal homegardens. *Food and Chemical Toxicology, 50*(3–4), 829–834. https://doi.org/10.1016/j.fct.2011.11.045

Pinheiro, W. M. (2015). Elaboração de sistema sinérgico visando aplicações em nanobiotecnologia, baseado em microesferas de polímeros naturais contendo berberina e nanopartículas de ouro associada a doxorrubicina. In *Dissertação*. Universidade de Brasília.

Prieto, M. A., & Vázquez, J. A. (2014). A Time-Dose Model to Quantify the Antioxidant Responses of the Oxidative Hemolysis Inhibition Assay (OxHLIA) and Its Extension to Evaluate Other Hemolytic Effectors. *BioMed Research International, 2014*, 1–15. https://doi.org/10.1155/2014/632971

Rasoulzadeh, F., Jabary, H. N., Naseri, A., & Rashidi, M. R. (2009). Fluorescence quenching study of quercetin interaction with bovine milk xanthine oxidase. *Spectrochimica Acta Part A: Molecular and Biomolecular Spectroscopy, 72*(1), 190–193. https://doi.org/10.1016/J.SAA.2008.09.021

Rheder, D. T., Guilger, M., Bilesky-José, N., Germano-Costa, T., Pasquoto-Stigliani, T., Gallep, T. B. B., Grillo, R., Carvalho, C. dos S., Fraceto, L. F., & Lima, R. (2018). Synthesis of biogenic silver nanoparticles using Althaea officinalis as reducing agent: evaluation of toxicity and ecotoxicity. *Scientific Reports*, *8*(1). https://doi.org/10.1038/s41598-018-30317-9.

Rocha, F., Yumi Sugahara, L., Leimann, F. V., de Oliveira, S. M., da Silva Brum, E., Calhelha, R. C., Barreiro, M. F., Ferreira, I. C. F. R., Porto Ineu, R., & Gonçalves, O. H. (2018). Nanodispersions of beta-carotene: Effects on antioxidant enzymes and cytotoxic properties. *Food and Function, 9*(7), 3698–3706. https://doi.org/10.1039/c8fo00804c

Sales, I. M. S., Sousa Barbosa, J., Sousa dos Santos, F. K., Cavalcanti Carneiro da Silva, F., Pinheiro Ferreira, P. M., de Castro e Sousa, J. M., & Peron, A. P. (2017). Acute Toxicity of Grape, Plum and Orange Synthetic Food Flavourings Evaluated in in vivo Test Systems. *Food Technology and Biotechnology*, *55*(1), 131–137. https://doi.org/10.17113/ftb.55.01.17.4770.

Salehi, B., Stojanović-Radić, Z., Matejić, J., Sharifi-Rad, M., Anil Kumar, V, N., … Sharifi-Rad, J. (2019). The therapeutic potential of curcumin: A review of clinical trials. *European Journal of Medicinal Chemistry, 163*, 527–545. https://doi.org/10.1016/j.ejmech.2018.12.016

Santos, P. D. D. F., Coqueiro, A., Brum, E. D. S., Oliveira, S. M., Leimann, F. V., Ineu, R. P., Bona, E., & Gonçalves, O. H. (2020). Endogenous antioxidant properties of curcuminoids from Curcuma longa L. obtained by a single-step extraction/nanoencapsulation approach. *Journal of Food Biochemistry.*. https://doi.org/10.1111/jfbc.13531

Sarraf, M., Beig Babaei, A., & Naji-Tabasi, S. (2019). Investigating functional properties of barberry species: An overview. *Journal of the Science of Food and Agriculture, 99*(12), 5255–5269. https://doi.org/10.1002/jsfa.9804

Schittny, A., Huwyler, J., & Puchkov, M. (2020). Mechanisms of increased bioavailability through amorphous solid dispersions: A review. *Drug Delivery, 27*(1), 110–127. https://doi.org/10.1080/10717544.2019.1704940

Schwaab, M., Biscaia, E. C., Monteiro, J. L., & Pinto, J. C. (2008). Nonlinear parameter estimation through particle swarm optimization. *Chemical Engineering Science, 63*(6), 1542–1552. https://doi.org/10.1016/J.CES.2007.11.024

Sharma, R. (2012). *Enzyme Inhibition and Bioapplications*. BoD – Books on Demand.

Shrimal, P., Jadeja, G., Naik, J., & Patel, S. (2019). Continuous microchannel precipitation to enhance the solubility of telmisartan with poloxamer 407 using Box-Behnken design approach. *Journal of Drug Delivery Science and Technology, 53*, Article 101225. https://doi.org/10.1016/j.jddst.2019.101225

Silva, J. T. D. P., Silva, A. C. D., Geiss, J. M. T., de Araújo, P. H. H., Becker, D., Bracht, L., Leimann, F. V., Bona, E., Guerra, G. P., & Gonçalves, O. H. (2017). Analytical validation of an ultraviolet–visible procedure for determining lutein concentration and application to lutein-loaded nanoparticles. *Food Chemistry, 230*. https://doi.org/10.1016/j.foodchem.2017.03.059

Sá, I. S., Peron, A. P., Leimann, F. V., Bressan, G. N., Krum, B. N., Fachinetto, R., Pinela, J., Calhelha, R. C., Barreiro, M. F., Ferreira, I. C. F. R., Gonçalves, O. H., & Ineu, R. P. (2019). In vitro and in vivo evaluation of enzymatic and antioxidant activity, cytotoxicity and genotoxicity of curcumin-loaded solid dispersions. *Food and Chemical Toxicology*, *125*(December 2018), 29–37. https://doi.org/10.1016/j.fct.2018.12.037.

Silva, J. T. do P., Geiss, J. M. T., Oliveira, S. M., Brum, E. da S., Sagae, S. C., Becker, D., Leimann, F. V., Ineu, R. P., Guerra, G. P., & Gonçalves, O. H. (2017). Nanoencapsulation of lutein and its effect on mice's declarative memory. *Materials Science and Engineering C, 76*, 1005–1011. https://doi.org/10.1016/j.msec.2017.03.212.

Silva, T. de S., Silva, A. P. S. e., de Almeida Santos, A., Ribeiro, K. G., Souza, D. C. de, Bueno, P. A. A., Marques, M. M. M., Almeida, P. M. de, & Peron, A. P. (2020). Cytotoxicity, Genotoxicity, and Toxicity of Plant Biostimulants Produced in Brazil: Subsidies for Determining Environmental Risk to Non-Target Species. *Water, Air, & Soil Pollution*, *231*(5), 233. https://doi.org/10.1007/s11270-020-04614-x.

Singh, A. K., Singh, S. K., Nandi, M. K., Mishra, G., Maurya, A., Rai, A., Rai, G. K., Awasthi, R., Sharma, B., & Kulkarni, G. T. (2019). Berberine: A Plant-derived Alkaloid with Therapeutic Potential to Combat Alzheimer's disease. *Central Nervous System Agents in Medicinal Chemistry, 19*(3), 154–170. https://doi.org/10.2174/1871524919666190820160053

Singh, A. K., Singh, S. S., Rathore, A. S., Singh, S. P., Mishra, G., Awasthi, R., Mishra, S. K., Gautam, V., & Singh, S. K. (2021). Lipid-Coated MCM-41 Mesoporous Silica Nanoparticles Loaded with Berberine Improved Inhibition of Acetylcholine Esterase and Amyloid Formation. *ACS Biomaterials Science and Engineering, 7*(8), 3737–3753. https://doi.org/10.1021/acsbiomaterials.1c00514

Sobral, F., Sampaio, A., Falcão, S., Queiroz, M. J. R. P., Calhelha, R. C., Vilas-Boas, M., & Ferreira, I. C. F. R. (2016). Chemical characterization, antioxidant, anti-inflammatory and cytotoxic properties of bee venom collected in Northeast Portugal. *Food and Chemical Toxicology*. https://doi.org/10.1016/j.fct.2016.06.008

Souza, A. H. P., Corrêa, R. C. G., Barros, L., Calhelha, R. C., Santos-Buelga, C., Peralta, R. M., Bracht, A., Matsushita, M., & Ferreira, I. C. F. R. (2015). Phytochemicals and bioactive properties of Ilex paraguariensis: An in-vitro comparative study between the whole plant, leaves and stems. *Food Research International, 78*, 286–294. https://doi.org/10.1016/j.foodres.2015.09.032

Su, T., Xie, S., Wei, H., Yan, J., Huang, L., & Li, X. (2013). Synthesis and biological evaluation of berberine–thiophenyl hybrids as multi-functional agents: Inhibition of acetylcholinesterase, butyrylcholinesterase, and Aβ aggregation and antioxidant activity. *Bioorganic & Medicinal Chemistry, 21*(18), 5830–5840. https://doi.org/10.1016/j.bmc.2013.07.011

Takebayashi, J., Iwahashi, N., Ishimi, Y., & Tai, A. (2012). Development of a simple 96-well plate method for evaluation of antioxidant activity based on the oxidative haemolysis inhibition assay (OxHLIA). *Food Chemistry, 134*(1), 606–610. https://doi.org/10.1016/j.foodchem.2012.02.086

Ventura-Camargo, B. de C., de Angelis, D. de F., & Marin-Morales, M. A. (2016). Assessment of the cytotoxic, genotoxic and mutagenic effects of the commercial black dye in Allium cepa cells before and after bacterial biodegradation treatment. *Chemosphere*, *161*, 325–332. https://doi.org/10.1016/j.chemosphere.2016.06.085.

Wang, L., Zhou, B. Q., Li, Y. H., Jiang, Q. Q., Cong, W. H., Chen, K. J., … Wu, Z. Z. (2023). Lactoferrin modification of berberine nanoliposomes enhances the neuroprotective effects in a mouse model of Alzheimer's disease. *Neural Regeneration Research, 18*(1), 226–232. https://doi.org/10.4103/1673-5374.344841

Wetwitayaklung, P., Limmatvapirat, C., Phaechamud, T., & Keokitichai, S. (2007). Kinetics of Acetylcholinesterase Inhibition of Quisqualis indica Linn. Flower Extract. *Science, Engineering and Health Studies, 1*(2), 20–28.

Xue, M., Yang, M., Zhang, W., Li, X., Gao, D., Ou, Z., Li, Z., Li, X., Liu, S., & Yang, S. (2013). Characterization, pharmacokinetics, and hypoglycemic effect of berberine loaded solid lipid nanoparticles. *International Journal of Nanomedicine, 4677*. https://doi.org/10.2147/IJN.S51262

Xue, M., Zhang, L., Yang, M., Zhang, W., Li, X., Ou, Z., Li, Z., Liu, S., Li, X., & Yang, S. (2015). Berberine-loaded solid lipid nanoparticles are concentrated in the liver and ameliorate hepatosteatosis in db/db mice. *International Journal of Nanomedicine, 10*, 5049. https://doi.org/10.2147/IJN.S84565

Yiannopoulou, K. G., & Papageorgiou, S. G. (2020). Current and Future Treatments in Alzheimer Disease: An Update. *Journal of Central Nervous System Disease*, *12*, 117957352090739. https://doi.org/10.1177/1179573520907397.

Yuan, N.-N., Cai, C.-Z., Wu, M.-Y., Su, H.-X., Li, M., & Lu, J.-H. (2019). Neuroprotective effects of berberine in animal models of Alzheimer's disease: A systematic review of pre-clinical studies. *BMC Complementary and Alternative Medicine, 19*(1), 109. https://doi.org/10.1186/s12906-019-2510-z

Zhang, Y., Cui, Y. L., Gao, L. N., & Jiang, H. L. (2013). Effects of β-cyclodextrin on the intestinal absorption of berberine hydrochloride, a P-glycoprotein substrate. *International Journal of Biological Macromolecules, 59*, 363–371. https://doi.org/10.1016/j.ijbiomac.2013.04.074

Zhang, Z., Chen, Y., Deng, J., Jia, X., Zhou, J., & Lv, H. (2014b). Solid dispersion of berberine–phospholipid complex/TPGS 1000/SiO2: Preparation, characterization and in vivo studies. *International Journal of Pharmaceutics, 465*(1–2), 306–316. https://doi.org/10.1016/j.ijpharm.2014.01.023

Zhao, C., Cai, Y., He, X., Li, J., Zhang, L., Wu, J., Zhao, Y., Yang, S., Li, X., Li, W., & Liang, G. (2010). Synthesis and anti-inflammatory evaluation of novel mono-carbonyl analogues of curcumin in LPS-stimulated RAW 264.7 macrophages. *European Journal of Medicinal Chemistry, 45*(12), 5773–5780. https://doi.org/10.1016/j.ejmech.2010.09.037

Zhaojie, M., Ming, Z., Shengnan, W., Xiaojia, B., Hatch, G. M., Jingkai, G., & Li, C. (2014). Amorphous solid dispersion of berberine with absorption enhancer demonstrates a remarkable hypoglycemic effect via improving its bioavailability. *International Journal of Pharmaceutics, 467*(1–2), 50–59. https://doi.org/10.1016/j.ijpharm.2014.03.017